THE JOURNAL OF BIOLOGICAL CHEMISTRY VOL. 286, NO. 28, pp. 25171–25186, July 15, 2011

Identification of the PDZ3 Domain of the Adaptor Protein PDZK1 as a Second, Physiologically Functional Binding Site for the C Terminus of the High Density Lipoprotein Receptor Scavenger Receptor Class B Type I*

Received for publication, March 22, 2011, and in revised form, April 21, 2011 Published, JBC Papers in Press, May 20, 2011, DOI 10.1074/jbc.M111.242362

Olivier Kocher[‡1], Gabriel Birrane[§], Ayce Yesilaltay[¶], Sharon Shechter[‡], Rinku Pal[‡], Kathleen Daniels[‡], and Monty Krieger[¶]

From the [‡]Department of Pathology and Center for Vascular Biology Research and [§]Division of Experimental Medicine, Beth Israel Deaconess Medical Center, Harvard Medical School, Boston, Massachusetts 02215 and the [¶]Department of Biology, Massachusetts Institute of Technology, Cambridge, Massachusetts 02139

The normal expression, cell surface localization, and function of the murine high density lipoprotein receptor scavenger receptor class B type I (SR-BI) in hepatocytes *in vivo*, and thus normal lipoprotein metabolism, depend on its four PDZ domain (PDZ1–PDZ4) containing cytoplasmic adaptor protein PDZK1. Previous studies showed that the C terminus of SR-BI ("target peptide") binds directly to PDZ1 and influences hepatic SR-BI protein expression. Unexpectedly an inactivating mutation in PDZ1 ($Tyr^{20} \rightarrow Ala$) only partially, rather than completely, suppresses the ability of PDZK1 to control hepatic SR-BI. We used isothermal titration calorimetry to show that PDZ3, but not PDZ2 or PDZ4, can also bind the target peptide (K_d = 37.0 μM), albeit with ~10-fold lower affinity than PDZ1. This binding is abrogated by a $Tyr^{253} \rightarrow Ala$ substitution. Comparison of the 1.5-Å resolution crystal structure of PDZ3 with its bound target peptide (^{505}QEAKL^{509}) to that of peptide-bound PDZ1 indicated fewer target peptide stabilizing atomic interactions (hydrogen bonds and hydrophobic interactions) in PDZ3. A double ($Tyr^{20} \rightarrow Ala$ (PDZ1) + $Tyr^{253} \rightarrow Ala$ (PDZ3)) substitution abrogated all target peptide binding to PDZK1. *In vivo* hepatic expression of a singly substituted ($Tyr^{253} \rightarrow Ala$ (PDZ3)) *PDZK1* transgene (Tg) was able to correct all of the SR-BI-related defects in *PDZK1* knock-out mice, whereas the doubly substituted [$Tyr^{20} \rightarrow Ala$ (PDZ1) + $Tyr^{253} \rightarrow Ala$ (PDZ3)]Tg was unable to correct these defects. Thus, we conclude that PDZK1-mediated control of hepatic SR-BI requires direct binding of the SR-BI C terminus to either the PDZ1 or PDZ3 domains, and that binding to both domains simultaneously is not required for PDZK1 control of hepatic SR-BI.

The expression and function of numerous proteins, including cell surface receptors, is controlled, at least in part, by interacting cytoplasmic adaptor proteins. These adaptors can play essential roles in regulating the functions of their targets, including signal transduction (1). PDZ (PSD-95/Discs-large/ZO-1) domains are a family of protein interaction domains (~250 in the human genome) found in over 100 proteins and can interact with and regulate the functions of a number of membrane-associated proteins (2). As PDZ domain-containing proteins often contain more than one PDZ domain, they are able to serve as scaffolds that can organize multiprotein complexes and thus influence cellular function. PDZK1 is a 519-amino acid cytoplasmic protein containing four PDZ domains (PDZ1–PDZ4) involved in the regulation of several membrane-associated proteins, including ion channels and cell-surface receptors (3, 4). Indeed, PDZK1 plays a major role in regulating the expression, localization, and function of the HDL-receptor scavenger receptor class B type I (SR-BI)[2] in a tissue-specific manner (5).

SR-BI is a 509-amino acid integral membrane protein with a large extracellular loop, two transmembrane domains, and very short cytoplasmic N and C termini (6). It plays a major role in the transfer of cholesterol from extracellular HDL particles to the cytoplasm of numerous cell types by selective uptake. Inactivation of the *SR-BI* gene in mice is characterized by a marked increase in plasma cholesterol (~2.2-fold) in the form of large HDL particles (7). In *apoE* knock-out (KO) mice that spontaneously develop aortic atherosclerosis (8, 9), SR-BI expression prevents the development of occlusive coronary artery disease, myocardial infarction, heart dysfunction, and premature death (10).

Inactivation of the *PDZK1* gene in mice (*PDZK1* KO) results in suppression of almost all (~95%) SR-BI protein expression in hepatocytes, a less dramatic decrease (~50%) of SR-BI expression in the small intestines, yet no change of expression in macrophages (11) and steroidogenic organs such as the adrenal cortex, ovary, and testis (5). *PDZK1* KO mice exhibit elevated plasma cholesterol levels (~1.7-fold), in the form of large abnormal HDL particles (5). These findings are similar to, but not as severe as, those observed in *SR-BI* KO mice (7). Because of their role in the regulation of lipoprotein metabolism, both SR-BI and PDZK1 are atheroprotective (10–13).

* This work was supported, in whole or in part, by National Institutes of Health Grants HL077780 (to O. K.), HL52212 and HL66105 (to M. K.).

[1] To whom correspondence should be addressed: Dept. of Pathology and Center for Vascular Biology Research, Beth Israel Deaconess Medical Center, Harvard Medical School, 330 Brookline Ave., Boston, MA 02215. Tel.: 617-667-3598; Fax: 617-667-3591; E-mail: okocher@bidmc.harvard.edu.

[2] The abbreviations used are: SR-BI, scavenger receptor class B type I; KO, knockout; CBL, carboxylate binding loop; PEG, polyethylene glycol; ITC, isothermal titration calorimetry; Tg, transgene.

Initially, SR-BI was shown to bind via its C terminus to the first, N-terminal PDZ domain of PDZK1 (PDZ1) and yeast two-hybrid experiments indicated that the PDZ1 domain was the only PDZ domain in PDZK1 that interacts with the C-terminal region of SR-BI (14). The precise function(s), if any, of PDZ2, PDZ3, and PDZ4 with regard to the control of SR-BI remained unclear. The importance of the C terminus of SR-BI for SR-BI/PDZK1 interaction was confirmed when Silver showed that removal of the C-terminal Leu^{509} from SR-BI prevented their binding and interfered with the surface expression of SR-BI in hepatocytes (15). Studies of PDZK1 variants with nested C-terminal deletions expressed in the livers of *PDZK1* KO and wild-type mice *in vivo* have provided additional insights into the PDZ domain roles of PDZK1 in controlling hepatic SR-BI (16, 17). Hepatic overexpression of the PDZ1 domain alone in PDZK1 KO mice is unable to complement their SR-BI defects (17). Analysis of additional deletion constructs established that all four PDZ domains of PDZK1 are necessary for normal expression and function of endogenous hepatic SR-BI (16). Hepatic overexpression of the PDZ1 domain alone in WT mice overcame the activity of the endogenous hepatic PDZK1 (dominant-negative effect), presumably by binding directly to the C terminus of SR-BI and thus preventing the binding of intact endogenous PDZK1 (17).

We were surprised, therefore, to find that hepatic overexpression in *PDZK1* KO mice of a mutant, full-length *PDZK1* transgene, in which the PDZ1 domain was inactivated, corrected hepatic SR-BI protein expression levels, and partially restored to normal its cell membrane localization and plasma cholesterol levels (18). The inactivation of PDZ1, loss of binding to the C terminus SR-BI, was a consequence of a $Tyr^{20} \rightarrow$ Ala substitution in the target peptide of the PDZ1 carboxylate binding loop (CBL). Therefore, we postulated that there might be additional binding sites within PDZK1 that bind SR-BI and mediate productive SR-BI-PDZK1 interaction previously attributed exclusively to the binding of PDZ1 to the C terminus of SR-BI.

Here, we generated recombinant proteins corresponding to each of the four PDZ domains of PDZK1 and identified a second binding site for the C terminus of SR-BI in the third PDZ domain (PDZ3). Binding of the C terminus of SR-BI to PDZ3, which exhibits lower affinity than to PDZ1, is inactivated by a $Tyr^{253} \rightarrow$ Ala amino acid substitution within the CBL of PDZ3. In addition, we generated full-length wild-type and mutated PDZK1 recombinant proteins containing either a single $Tyr^{20} \rightarrow$ Ala (PDZ1) or a double $Tyr^{20} \rightarrow$ Ala (PDZ1) + $Tyr^{253} \rightarrow$ Ala (PDZ3) amino acid substitution(s). Full-length, wild-type PDZK1 exhibits high and low affinity binding sites for the C terminus of SR-BI. Although the $Tyr^{20} \rightarrow$ Ala (PDZ1) substitution inactivated the high affinity binding site only, the $Tyr^{20} \rightarrow$ Ala (PDZ1) + $Tyr^{253} \rightarrow$ Ala (PDZ3) double substitution resulted in complete inactivation of the C terminus of SR-BI binding to PDZK1. We also determined the high-resolution crystal structure of wild-type PDZ3 alone and in complex with its SR-BI target peptide to better understand the interaction and the effects of the amino acid substitutions on target peptide binding *in vitro*. In addition, we incorporated several amino acid substitution mutations into full-length PDZK1 expression constructs and used them to generate transgenic WT and *PDZK1* KO mice with liver-specific expression of the transgenes, including [$Tyr^{253} \rightarrow$ Ala (PDZ3)]Tg, and a double mutant [$Tyr^{20} \rightarrow$ Ala (PDZ1) + $Tyr^{253} \rightarrow$ Ala (PDZ3)]Tg. We previously showed that a mutant *PDZK1* transgene with an inactivating mutation in PDZ1 ($Tyr^{20} \rightarrow$ Ala) alone can almost completely correct the SR-BI-related defects in *PDZK1* KO mice (18). Here we show that the hepatic expression of [$Tyr^{253} \rightarrow$ Ala (PDZ3)]Tg was able to correct all of the SR-BI-related defects in *PDZK1* KO mice, whereas the doubly substituted [$Tyr^{20} \rightarrow$ Ala (PDZ1) + $Tyr^{253} \rightarrow$ Ala (PDZ3)]Tg was unable to correct these defects. Thus, we conclude that PDZK1 regulation of hepatic SR-BI requires direct binding of the C terminus of SR-BI to either the PDZ1 or PDZ3 domain, and that binding to both domains simultaneously is not required for the hepatic, PDZK1-dependent, SR-BI activities measured in this study.

EXPERIMENTAL PROCEDURES

Generation of Full-length PDZK1 cDNAs Encoding Proteins with Single and Double Amino Acid Substitutions—Vectors encoding PDZK1 with single residue substitutions $Phe^{145} \rightarrow$ Ala (PDZ2), $Tyr^{253} \rightarrow$ Ala (PDZ3), and $Tyr^{388} \rightarrow$ Ala (PDZ4), as well as the double substitution ($Tyr^{20} \rightarrow$ Ala + $Tyr^{253} \rightarrow$ Ala) were produced using a previously described wild-type PDZK1/pLiv-LE6 recombinant plasmid (17) and the QuikChange site-directed mutagenesis kit (Stratagen) according to the manufacturer's protocol. Oligonucleotide primers containing the corresponding mutations were synthesized and PAGE purified by Integrated DNA Technologies. The sequences of the resulting plasmids were confirmed by DNA sequencing.

Recombinant Protein Production and Purification—The cDNAs encoding full-length wild-type and single and double residue-substituted PDZK1 in pLiv-LE6 (see above) were used as templates to generate PCR products corresponding to each of the four individual PDZ domains in wild-type PDZK1 (PDZ1–PDZ4), as well as PDZ3 containing the $Tyr^{253} \rightarrow$ Ala substitution. These products were cloned into pGEX-4T-3 and expressed in *Escherichia coli* JM109 cells to produce glutathione *S*-transferase fusion proteins. In addition, DNA fragments encoding the wild-type full-length PDZK1 protein or full-length PDZK1 containing either a single $Tyr^{20} \rightarrow$ Ala substitution or the ($Tyr^{20} \rightarrow$ Ala (PDZ1) + $Tyr^{253} \rightarrow$ Ala (PDZ3)) double substitution were generated by restriction enzyme (BamHI/XhoI) digestion of the corresponding PDZK1/pLiv-LE6 plasmids and cloned into pGEX-4T-3 and expressed in *E. coli* JM109 cells to produce glutathione *S*-transferase fusion proteins. The expressed proteins were purified on glutathione-Sepharose 4B (GE Healthcare) and released by digestion with thrombin. The recombinant proteins contained the following residues from PDZK1: PDZ1, 7–116; PDZ2, 133–242; PDZ3, 241–348; and PDZ4, 376–484. Each isolated recombinant protein (109 to 111 residues total) contained a Gly-Ser dipeptide at the N termini that is not normally present in PDZK1 because it is encoded by the cloning vector. The recombinant proteins were further purified by fast protein liquid chromatography (FPLC) using Superdex S-75 or Superdex S-200 columns (GE Healthcare) in a buffer containing 150 mM NaCl, 25 mM Tris, pH 8.0, at 4 °C under reducing conditions (0.5 mM tris(2-car-

boxyethyl)phosphine)), and were shown to be homogeneous using SDS-PAGE.

Isothermal Titration Calorimetry (ITC)—Binding of recombinant proteins to the C-terminal heptapeptide of SR-BI (^{503}VLQEAKL^{509}, "target peptide") was measured using a VP-ITC microcalorimeter (GE Healthcare). The SR-BI peptide was synthesized and purified by HPLC at the Tufts University Core Facility (Boston). Briefly, 0.3–1.0 mM of the target peptide was titrated against the four individual PDZ domain-derived or full-length wild-type or mutated PDZK1 recombinant proteins at concentrations of 0.03 mM in a buffer containing 150 mM NaCl, 25 mM Tris, pH 8.0, at 20 °C under reducing conditions (0.5 mM tris(2-carboxyethyl)phosphine). Titration curves were analyzed and K_d values were determined using ORIGIN 7.0 software (Origin Lab) with baseline correction. Protein and peptide concentrations were determined by quantitative amino acid analysis (Dana Farber Molecular Biology Core Facility) and absorption spectroscopy (280 nm).

Crystallography—A PCR-generated DNA fragment encoding the PDZ3 recombinant protein without ligand (residues 238–323 of PDZK1, including the third PDZ domain of PDZK1 (residues 241–319), 3 residues from the region of the protein between the PDZ2 and PDZ3 domain (interdomain residues 238–240), and 4 residues from the region of the protein between the PDZ3 and PDZ4 domains (interdomain residues 320–323) was cloned into pGEX-4T-3 and expressed in *E. coli* JM109 cells to produce glutathione *S*-transferase fusion proteins. The recombinant protein was purified on glutathione-Sepharose 4B, released from GST using thrombin protease digestion, and further purified by FPLC using a Superdex S-75 column in a buffer containing 150 mM NaCl, 25 mM Tris, pH 8.0, at 4 °C under reducing conditions (0.5 mM tris(2-carboxyethyl)phosphine)). The isolated recombinant protein (95 residues total) contains an additional 2 residues (Gly-Ser) at the N terminus and 7 amino acids at the carboxyl terminus (LERPHRD) encoded by the cloning vector, which are not normally present in PDZK1. After initial screening for optimal crystallization conditions using the Classic suite (Qiagen), PDZ3 at 1 mM concentration was crystallized by the sitting drop vapor diffusion method at 18 °C in a well containing 0.2 M zinc acetate, 0.1 M sodium cacodylate, pH 6.2, 15% (w/v) PEG 3350, and 10% (w/v) ethylene glycol (the initial buffer composition of the protein drop included 50% FPLC buffer (150 mM NaCl, 25 mM Tris, pH 8.0, and 0.5 mM tris(2-carboxyethyl)phosphine) and 50% of 0.2 M zinc acetate, 0.1 M sodium cacodylate, pH 6.2, 15% (w/v) PEG 3350, and 10% (w/v) ethylene glycol). Crystals were flash frozen directly in liquid nitrogen. Diffraction data were collected on beamline X12C at the National Synchrotron Light Source (Brookhaven National Laboratory, NY). The crystals belong to space group $P4_32_12$ with unit cell dimensions of $a = b = 69.910$ and $c = 37.659$ Å.

In addition, a PCR-generated DNA fragment encoding the chimeric PDZ3-SR-BI recombinant protein (residues 241–322 of PDZK1, including PDZ3 (residues 241–319), 3 residues from the region of the protein between the PDZ3 and PDZ4 domain (interdomain residues 320–322) and, fused to the C terminus of this interdomain segment, the five carboxyl-terminal amino acids of SR-BI (^{505}QEAKL^{509}), was cloned into pGEX-4T-3 and expressed in *E. coli* JM109 cells to produce a glutathione *S*-transferase fusion protein. The recombinant protein was purified on glutathione-Sepharose 4B, released from GST using thrombin digestion, and further purified by FPLC using a Superdex S-75 column. The isolated, recombinant protein (89 residues total) contains an additional 2 residues (Gly-Ser, from the cloning vector) at the N terminus not normally present in PDZK1. After the initial screening for optimal crystallization conditions using the Classic II suite (Qiagen), the PDZ3-SR-BI chimera at 1 mM concentration was crystallized by the sitting drop vapor diffusion method at 18 °C in a well containing 0.1 M citric acid, pH 3.5, and 25% (w/v) PEG 3350. Crystals were, after being briefly immersed into the mother liquor supplemented with 5% ethylene glycol, flash frozen directly in liquid nitrogen. Diffraction data were collected on beamline X12C at the National Synchrotron Light Source (Brookhaven National Laboratory, NY). The crystals belong to space group $P2_12_12_1$ with unit cell dimensions of $a = 47.638$, $b = 61.396$, and $c = 64.010$ Å. The data were reduced and merged using the HKL2000 suite (19). Data collection and processing statistics for both crystals are given in Table 1.

Structure Determination and Refinement—Because the crystallization of PDZ3 without ligand involved buffer containing 0.2 M zinc acetate, we postulated that zinc could be used for phasing. The PDZ3 structure without ligand was solved using single wavelength anomalous diffraction at the zinc edge. Four zinc atoms were located using the automated structure determination package SHELX (20). The PDZ3-SR-BI chimeric structure was solved by molecular replacement with Phaser (21) using the coordinates of PDZ3 without ligand as a search model. Refinement was carried out with REFMAC5 (22) and model building and addition of water molecules was performed manually using Coot (23). The atomic coordinates and structure factors have been deposited in the Protein Data Bank as entries 3R68 and 3R69.

Animals—All animal experiments were performed according to IACUC guidelines. All mice (25:75 FVB/N:129SvEV genetic background) were maintained on a normal chow diet (24) and ~6–8-week-old male mice were used for experiments. All procedures on transgenic and non-transgenic mice were performed in accordance with the guidelines of the Beth Israel Deaconess Medical Center and the Massachusetts Institute of Technology Committee on Animal Care.

Founder transgenic animals in an FVB/N genetic background were generated using the full-length PDZK1 (wild-type and mutant) pLiv-LE6 expression vectors described above. The pLIV-LE6 plasmid, kindly provided by Dr. John M. Taylor (Gladstone Institute of Cardiovascular Disease, University of California, San Francisco, CA), contains the promoter, first exon, first intron, and part of the second exon of the human *apoE* gene, and the polyadenylation sequence, and a part of the hepatic control region of the *apoE*/*C-I* gene locus (25). The transgenic expression vectors were linearized by SacII/SpeI digestion and the resulting 7.3-kb constructs were used to generate transgenic mice using standard procedures (26). Transgenic animals were identified by PCR performed on tail DNA using the following oligonucleotide primers: one at the 3′-end of the *PDZK1* cDNA (GCAGATGCCTGTTATAGAAGT-

GTGC) and one corresponding to the 3′-end of the human *apoE* gene sequence included in the cloning vector (AGCAGATGCGTGAAACTTGGTGA). Founders expressing *PDZK1* transgenic mutants were crossed with *PDZK1* KO mice (129SvEv background). Heterozygous pups expressing the transgenes were crossed with WT and PDZK1 KO mice to obtain transgenic and control non-transgenic WT and *PDZK1* KO mice, thus ensuring that the mixed genetic backgrounds of experimental and control mice in each founder line were matched. *PDZK1* KO mice were genotyped as previously described (24). Two independent founder lines for [$Phe^{145} \rightarrow Ala$]transgene (Tg), one founder line for [$Tyr^{253} \rightarrow Ala$]Tg, two independent founder lines for [$Tyr^{388} \rightarrow Ala$]Tg and three independent founder lines for double mutant [$Tyr^{20} \rightarrow Ala$ and $Tyr^{253} \rightarrow Ala$]Tg were generated.

Blood and Tissue Sampling, Processing, and Analysis—Plasma and liver samples were collected and processed and total plasma cholesterol levels and individual size-fractionated FPLC cholesterol profiles were obtained as previously described (17). Plasma cholesterol results presented here for transgenic mice are pooled from data collected from animals derived from the different founder transgenic animals because the results obtained were not significantly different between founders expressing the same transgene.

For immunoblotting, protein samples (~30 μg) from total liver lysates were fractionated by SDS-PAGE, transferred to nitrocellulose membranes, and incubated with either a rabbit polyclonal SR-BI antibody (mSR-$BI^{495-112}$) (1:1000) or a rabbit polyclonal PDZK1 antibody (1:30,000) (17), followed by an anti-rabbit IgG conjugated to horseradish peroxidase (Invitrogen, 1:10,000), and visualized by ECL chemiluminescence (GE Healthcare). Immunoblotting using a polyclonal anti-ϵ-COP antibody (1:5,000) (27) was used to control for small variations in loading. The relative amounts of proteins were determined quantitatively using a Kodak Image Station 440 CF and Kodak one-dimensional software.

Immunoperoxidase Analysis—Livers were harvested, fixed, frozen, and 5-μm sections were stained with the anti-mSR-$BI^{495-112}$ antibody and biotinylated anti-rabbit IgG, visualized by immunoperoxidase staining, and counterstained with Harris modified hematoxylin, as described previously (5).

Statistical Analysis—Data are shown as the mean ± S.D. Statistically significant differences were determined by either pairwise comparisons of values using the unpaired *t* test, with (if variances differed significantly) or without Welch's correction, or by one-way analysis of variance followed by the Tukey-Kramer multiple comparison post-test when comparing three or more variables. Mean values for experimental groups are considered statistically significantly different for $p < 0.05$ for both types of tests.

RESULTS

Identification by ITC of the PDZ3 Domain of PDZK1 as a Second Binding Site for the C Terminus of SR-BI—It is commonly accepted that SR-BI interacts via its cytoplasmic C terminus with the first PDZ domain of PDZK1 (PDZ1) (14, 18). This interaction is important for controlling the expression, localization, and function of SR-BI (5, 15–17, 28). However, recent experiments suggested the existence of additional binding sites for SR-BI within PDZK1. A $Tyr^{20} \rightarrow Ala$ substitution in the conserved carboxylate binding loop of PDZ1 fully blocks SR-BI C terminus binding to PDZ1 *in vitro* (18). Unexpectedly, when expressed in the livers of otherwise *PDZK1* null mice, a full-length *PDZK1* transgene containing a $Tyr^{20} \rightarrow Ala$ substitution (18) can partially restore SR-BI expression and function, including partially correcting the lipoprotein abnormalities observed in *PDZK1* KO mice (18). These results suggested that there might be additional sites on PDZK1 that can bind to SR-BI, perhaps via the C terminus of SR-BI, and mediate the activity regulation of PDZK1. To identify putative additional binding sites, we performed ITC experiments using a synthetic peptide corresponding to the 7 carboxyl-terminal amino acids of SR-BI (^{503}VLQEAKL^{509}) and recombinant proteins corresponding to the four individual PDZ domains of PDZK1: PDZ1 (most N-terminal), PDZ2, PDZ3, and PDZ4 (most C-terminal), prepared as described under "Experimental Procedures." These experiments confirmed the presence of a high affinity binding site for the SR-BI carboxyl-terminal peptide on PDZ1 (K_d of 3.6 ± 0.4 μM) (Fig. 1*A*) (18) and no detectable peptide binding to the PDZ2 or PDZ4 domains (Fig. 1, *B* and *E*). We also observed an additional lower affinity binding site (K_d of 37.0 ± 6.3 μM) on PDZ3 (Fig. 1*C*) that was completely disrupted by a $Tyr^{253} \rightarrow Ala$ substitution in its carboxylate-binding loop (Fig. 1*D*), a substitution analogous to the inactivating $Tyr^{20} \rightarrow Ala$ substitution in the PDZ1 domain (18).

To confirm the presence of two binding sites for SR-BI in full-length PDZK1, we produced full-length recombinant PDZK1 proteins (wild type (WT) and mutants) as described under "Experimental Procedures." Using ITC binding studies with the C-terminal peptide of SR-BI, we determined that peptide binding to WT PDZK1 was best fit by a two-site binding model (K_{d1} 1.2 ± 0.3 and K_{d2} 19.0 ± 4.1 μM, respectively, Fig. 2*A*). Introduction of a single $Tyr^{20} \rightarrow Ala$ substitution in the PDZ1 domain into full-length PDZK1 abrogated high affinity binding but retained the low affinity binding site (Fig. 2*B*, K_d 33.2 ± 6.0 μM, a value not significantly different for the individual PDZ3 domain (Fig. 1*C*)). We could not detect binding of the carboxyl-terminal peptide of SR-BI to the full-length PDZK1 containing both $Tyr^{20} \rightarrow Ala$ (PDZ1) and $Tyr^{253} \rightarrow Ala$ (PDZ3) substitutions (Fig. 2*C*). We conclude that the SR-BI C-terminal peptide can bind to PDZK1 via both PDZ1 (high affinity) and PDZ3 (low affinity) domains. It is possible that some differences in observed K_d values between individual domains and those domains when incorporated into the full-length PDZK1 protein may arise because of interdomain interactions in the full-length protein. The C-terminal SR-BI peptide binding to PDZ3 may be the source of the residual *in vivo* activity of the $Tyr^{20} \rightarrow Ala$ PDZK1 mutant (18).

Crystal Structures of PDZ3 Without and With Bound Target Peptide—We have determined the structure of PDZ3 in the absence and presence of its bound target peptide, the C terminus of SR-BI using two recombinant proteins. The first consists of a 95-residue protein containing the PDZ3 domain of PDZK1 (residues 241–319), 3 residues from the interdomain region between PDZ2 and PDZ3 (residues 238–240), 4 residues from the interdomain region between PDZ3 and PDZ4 (residues 320–323), and several residues encoded by the cloning vector

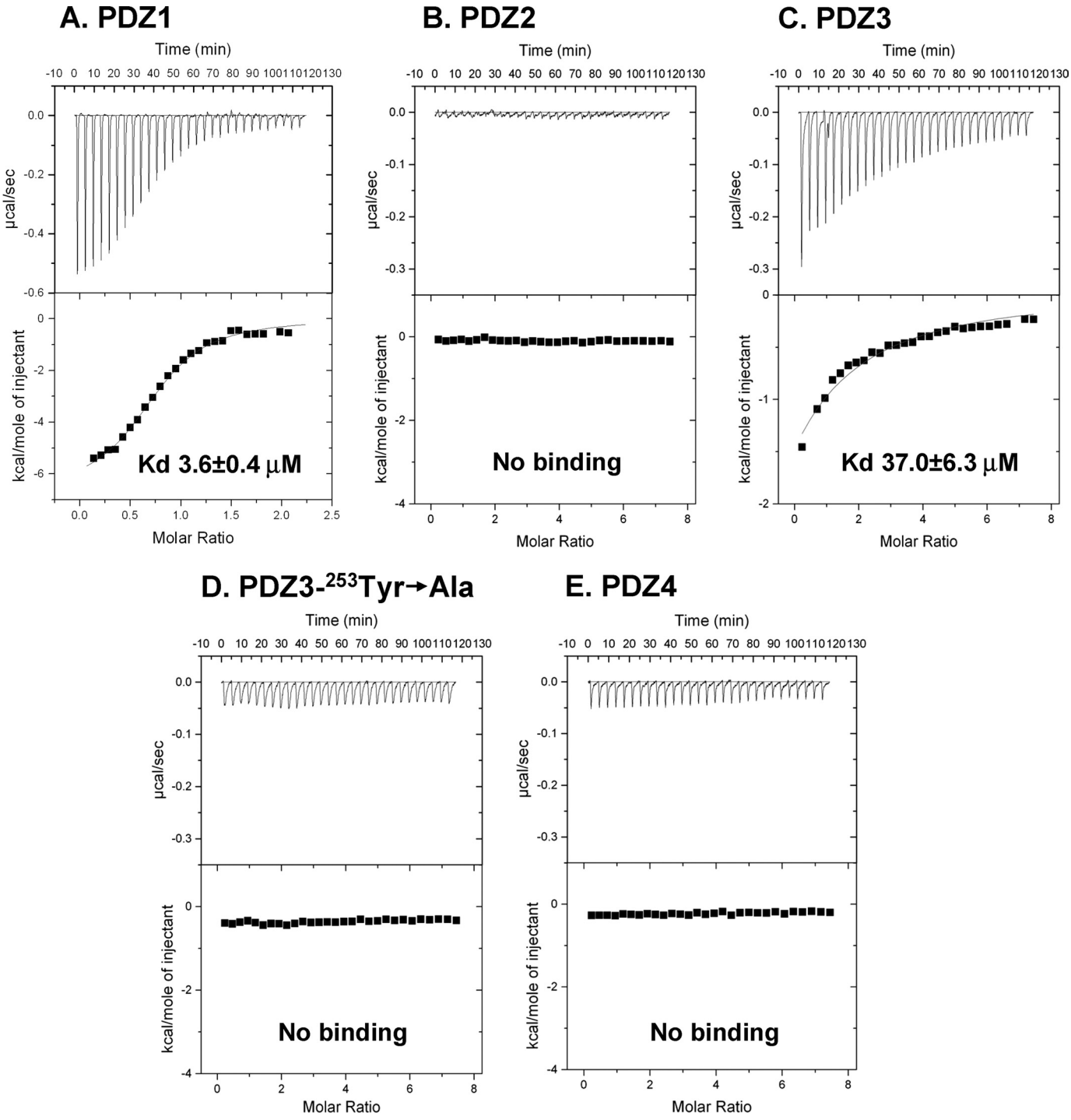

FIGURE 1. **Isothermal titration calorimetric analysis of the binding of a C-terminal peptide from SR-BI to individual recombinant PDZ domains of PDZK1.** The indicated individual recombinant wild-type and mutant PDZ domains (0.03 mM in 1.8 ml of 150 mM NaCl, 0.5 mM tris(2-carboxyethyl)phosphine, 25 mM Tris, pH 8.0) were placed in a titration cell and equilibrated at 20 °C: PDZ1 (*A*), PDZ2 (*B*), PDZ3 (*C*), PDZ3 containing a $Tyr^{253} \rightarrow Ala$ substitution (*D*), and PDZ4 (*E*). A solution containing 0.3 to 1.0 mM of the C-terminal heptapeptide from SR-BI, ^{503}VLQEAKL^{509}, was injected in 10-μl aliquots with an interval of 4 min between each addition to permit re-equilibration. Titration curves were analyzed and K_d values were determined using ORIGIN 7.0 software.

that are not present in PDZK1, including a glycine-serine dipeptide at the N terminus and a LERPHRD heptapeptide at the carboxyl terminus (Fig. 3*A*). Crystals of this protein without bound target peptide were grown and high resolution data were collected at the NSLS (Brookhaven National Laboratory). Because the crystallization buffer contained 0.2 M zinc acetate, we were able to use the zinc atoms incorporated into the crystal and single wavelength anomalous diffraction phasing to solve the structure (1.3-Å resolution), which had a final refined R_{cryst} and R_{free} factors of 13.1 and 15.7%, respectively (Table 1). The final model contains 699 protein atoms, 116 water molecules, 4 zinc, 5 chloride, 2 calcium, 2 acetate ions, and 1 ethylene glycol molecule. The high quality of the electron density map permitted unequivocal assignment of amino acid side chains, except

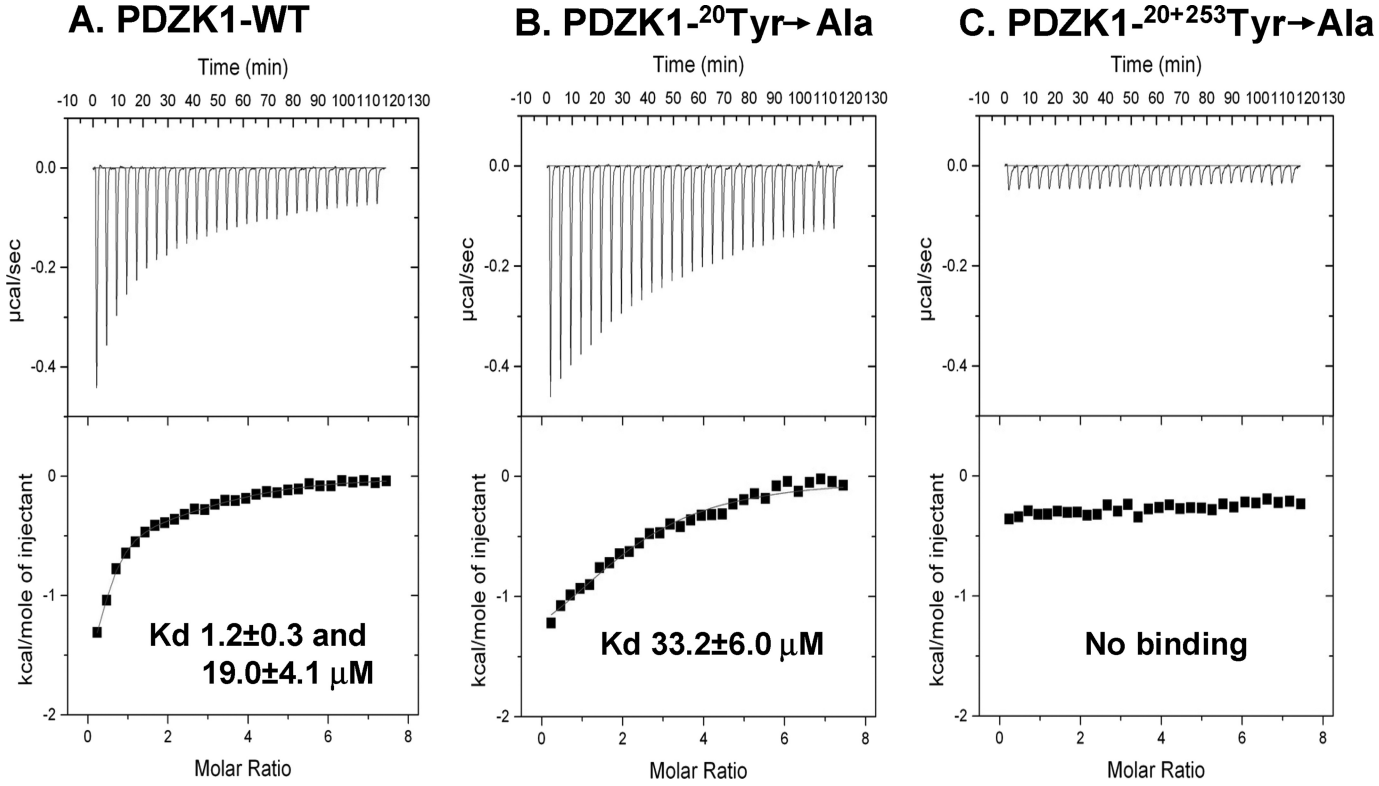

FIGURE 2. **Isothermal titration calorimetric analysis of the binding of a C-terminal peptide from SR-BI to full-length wild-type (*A*) and mutant (*B* and *C*) PDZK1 recombinant proteins.** The indicated recombinant, full-length WT (*A*) or mutant (single or double substitutions) (*B* and *C*) PDZK1 recombinant proteins (0.03 mM in 1.8 ml of 150 mM NaCl, 0.5 mM tris(2-carboxyethyl)phosphine, 25 mM Tris, pH 8.0) were placed in a titration cell and equilibrated at 20 °C. A solution containing 1.0 mM of the C-terminal heptapeptide from SR-BI, ^{503}VLQEAKL^{509}, was injected in 10-μl aliquots with an interval of 4 min between each addition to permit re-equilibration. Titration curves were analyzed and K_d values were determined using ORIGIN 7.0 software.

for a short disordered loop between the β2 and β3 strands, where the peptide chain linking residues 260 and 262 could not be assigned and was therefore not included in the final model. The tertiary structure of PDZ3 matches that previously described for many PDZ domains, a compact globular structure containing a six-stranded antiparallel β-barrel (β1–β6) flanked by two α-helices (α1 and α2) (Fig. 3*B*) (18, 29, 30). There is an unusual zinc-chloride-water chain containing 3 zinc, 3 chloride, and 5.5 water molecules (1 water molecule sits on the symmetry axis and is therefore shared between two PDZ3 molecules) (Fig. 3*C*). This chain fits into a groove between the β2-strand and the α2 helix interacting with them and the carboxylate binding loop (CBL) formed by Lys^{248}-Gly^{249}-Ser^{250}-Asn^{251}-Gly^{252}-Tyr^{253}-Gly^{254}-Phe^{255}-Tyr^{256}-Leu^{257} that connects the β1 and β2 strands (Fig. 3*C*). The zinc-chloride-water network promotes the dimerization of PDZ3 molecules within the crystal lattice (Fig. 3*D*), with a 2-fold rotation axis passing through the center of the water molecule labeled (W) that forms hydrogen bonds with zinc atoms, which in turn form hydrogen bonds with the side chains of His^{301} (length = 2.05 Å) and Asp^{302} (length = 2.02 Å) from adjacent, symmetry related molecules. The zinc-chloride-water chain sits in the groove that in PDZ domains normally binds their C-terminal target peptides (described below).

Our strategy to study the structure of PDZ3 with a bound target peptide was to crystallize and analyze a chimera of PDZ3 and the C terminus of SR-BI. This approach is based on that previously reported for the structural analyses of the human Na^+/H^+ exchanger regulatory factor PDZ1 bound to the cystic fibrosis transmembrane conductance regulator (31), the β_2-adrenergic and platelet-derived growth factor receptors (32), and the interaction of SR-BI with the PDZ1 domain of PDZK1 (18). We generated a second recombinant, chimeric protein, which included an N-terminal Gly-Ser dipeptide from the cloning vector, the third PDZ domain of PDZK1 (residues 241–319), and 3 residues from the interdomain region between PDZ3 and PDZ4 (residues 320–322) followed by the carboxyl-terminal 5 amino acids of SR-BI (^{505}QEAKL^{509} SR-BI numbering or alternatively $^{-4}$QEAKL^{0}) (Fig. 4*A*). Crystals were grown and high resolution synchrotron data were collected at the NSLS (Brookhaven National Laboratory). The space group of the complex ($P2_12_12_1$) was different from that of the target peptide-free structure ($P4_32_12$) described above. The structure was solved at 1.5-Å resolution by molecular replacement with PHASER (21) using the coordinates of the target peptide-free PDZ3 as the search model. The final values of the R_{cryst} and R_{free} factors were 20.0 and 22.6%, respectively (Table 1). The final model contains 1322 protein atoms, 141 water and 1 citrate molecules. The high quality of the electron density map (*e.g.* Fig. 4*C*) permitted unequivocal assignment of amino acid side chains, except for a short disordered loop between the β2 and β3 strands, containing residues 262 and 263, which could not be assigned with confidence and was therefore omitted from the model. Fig. 4*B* shows that in the crystal the SR-BI peptide (*yellow*) of one molecule interacts with the peptide binding pocket of the PDZ domain (*green*) of an adjacent molecule (two mole-

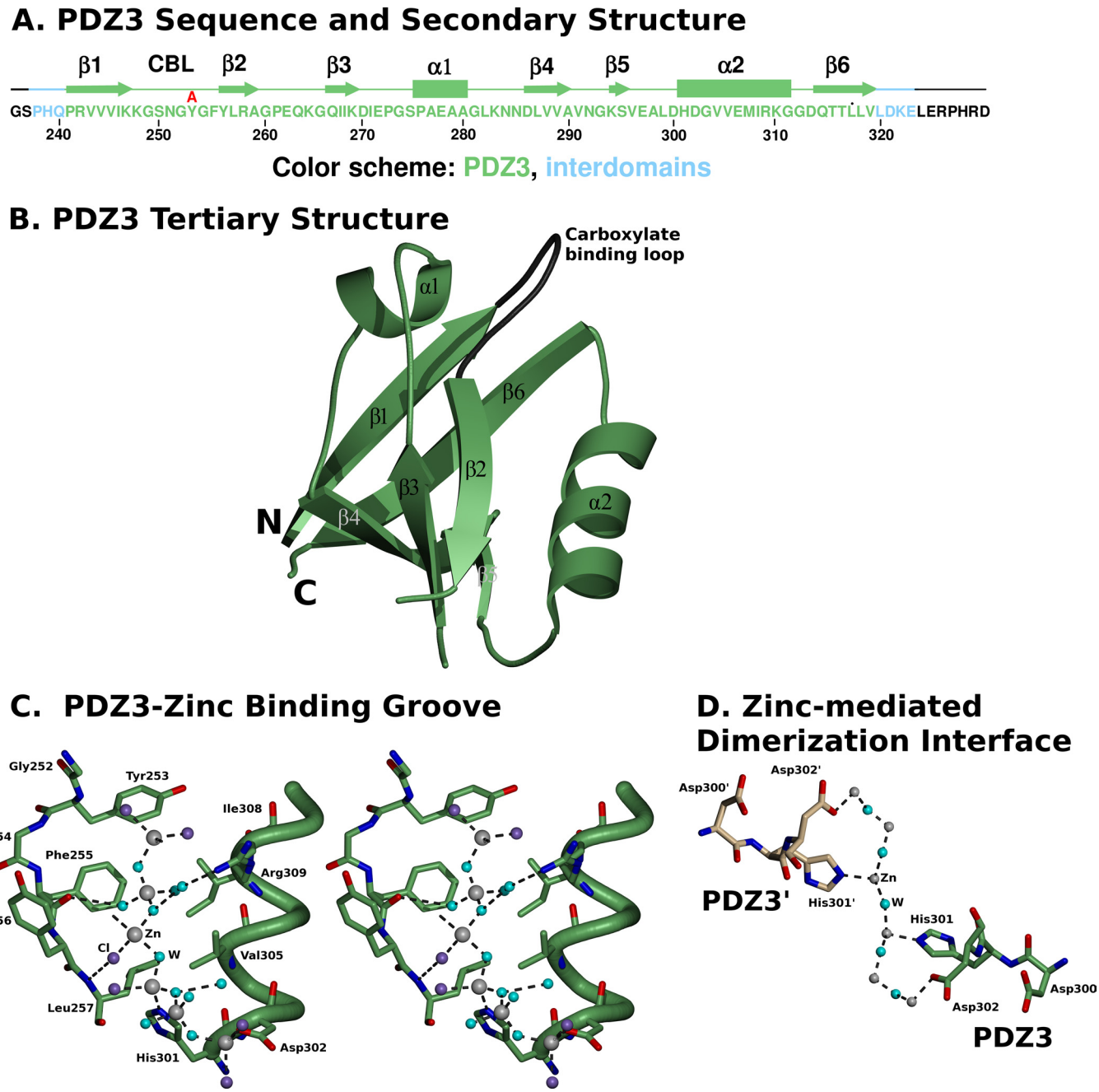

FIGURE 3. **X-ray crystal structure of PDZ3 without bound target peptide.** *A*, amino acid sequence of the recombinant protein used for crystallization: N-terminal Gly-Ser dipeptide derived from the cloning vector (*black*), partial interdomain segment (residues 238–240 (PDZK1 numbering), lies between the PDZ2 and PDZ3 domains, *blue*), PDZ3 domain (residues 241–319, *green*), partial interdomain segment (residues 320–323, lies between the PDZ3 and PDZ4 domains, *blue*), and 7 C-terminal residues derived from the cloning vector (*black*). Regions of secondary structure (β strands and α helices) determined from the structure and the CBL are indicated *above* the sequence, as is the single amino acid substitution ($Tyr^{253} \rightarrow Ala$) examined in this study (*red*). *B,* ribbon diagram showing the three-dimensional structure of PDZ3 (residues 241–319). The six β-strands ($\beta1$–$\beta6$), two α-helices ($\alpha1$–$\alpha2$), and carboxylate binding loop (*dark gray*) are indicated. The vector-derived residues are not shown. This figure was generated using POVScript (34) using the color scheme in *panel A*. *C,* stereo representation of the binding groove of PDZ3 (*green*) showing the zinc-chloride-water network: oxygen, *red*; nitrogen, *dark blue*; zinc, *gray spheres*; chloride, *violet spheres*; and water, *cyan spheres*. Hydrogen bonds are shown as *dashed lines*. The orientation is similar to that in *panel B*. *D,* representation of the zinc network-mediated dimerization of PDZ3 molecules. One PDZ3 molecule is colored *green*, whereas the adjacent symmetry-related PDZ3 molecule (*PDZ3′*) is colored *beige*.

cules, designated A and B, per asymmetric unit), resulting in an "infinite chain" of head-to-tail molecules that runs parallel to the crystallographic *c* axis. The interdomain sequence is shown in *blue*. Fig. 5*A* shows that the tertiary structure of PDZ3 (*green*) with its bound target peptide (C terminus of SR-BI, *yellow*) matches that of the target peptide-free (unbound) PDZ3 (Fig. 3*B*) and several other PDZ domains (29, 30). There is a well defined, extensive, hydrogen bonding network (*dashed lines* in Fig. 5, *B* and *C*) directly and indirectly connecting the target peptide, multiple regions of PDZ3, and bound water molecules. The carboxylate group of the target peptides of Leu^{0} makes hydrogen bonds with the amide nitrogens of Tyr^{253}, Gly^{254}, and

TABLE 1
Structure determination and refinement statistics of PDZ3 without bound target peptide and PDZ3-SR-BI target peptide chimera

	PDZ3	PDZ3-SR-BI
Data collection		
Space group	$P4_32_12$	$P2_12_12_1$
Unit cell (Å)	$a = b = 69.9$, $c = 37.7$	$a = 47.638$, $b = 61.396$, $c = 64.010$
Wavelength (Å)	1.075	0.978
Resolution (Å)[a]	100.0-1.2 (1.22-1.20)	50.0-1.5 (1.55-1.50)
Completeness (%)	97.0 (69.7)	94.5 (66.4)
Total observations	334,691	168,274
Unique observations	28,919	29,138
Redundancy	11.6 (4.4)	5.8 (2.2)
R_{sym}	6.9 (49.5)	4.5 (33.7)
$\langle I/\sigma(I)\rangle$	31.9 (2.2)	37.4 (2.4)
Refinement		
Resolution (Å)	33.2-1.3	23.9-1.5
R_{cryst} (%)	13.1	20.0
R_{free} (%)	15.7	22.6
Root mean square deviation bond lengths (Å)	0.014	0.018
Root mean square deviation bond angles (°)	1.607	1.718
Ramachandran plot		
Preferred/allowed/outliers (%)	98.9, 1.1, 0.0	92.6, 7.4, 0.0

[a] Values in parenthesis are for the highest resolution shell. $R_{sym} = \Sigma|I-\langle I\rangle|/\Sigma(I)$, where I is the observed integrated intensity, $\langle I\rangle$ is the average integrated intensity obtained from multiple measurements, and the summation is over all observable reflections. $R_{cryst} = \Sigma||F_{obs}| - k|F_{calc}||\Sigma|F_{obs}|$, where F_{obs} and F_{calc} are the observed and calculates structure factors, respectively. R_{free} is calculates as R_{cryst} using 5% of the reflection chosen randomly and omitted from the refinement calculations. Bond lengths and angles are root mean square deviations from ideal values.

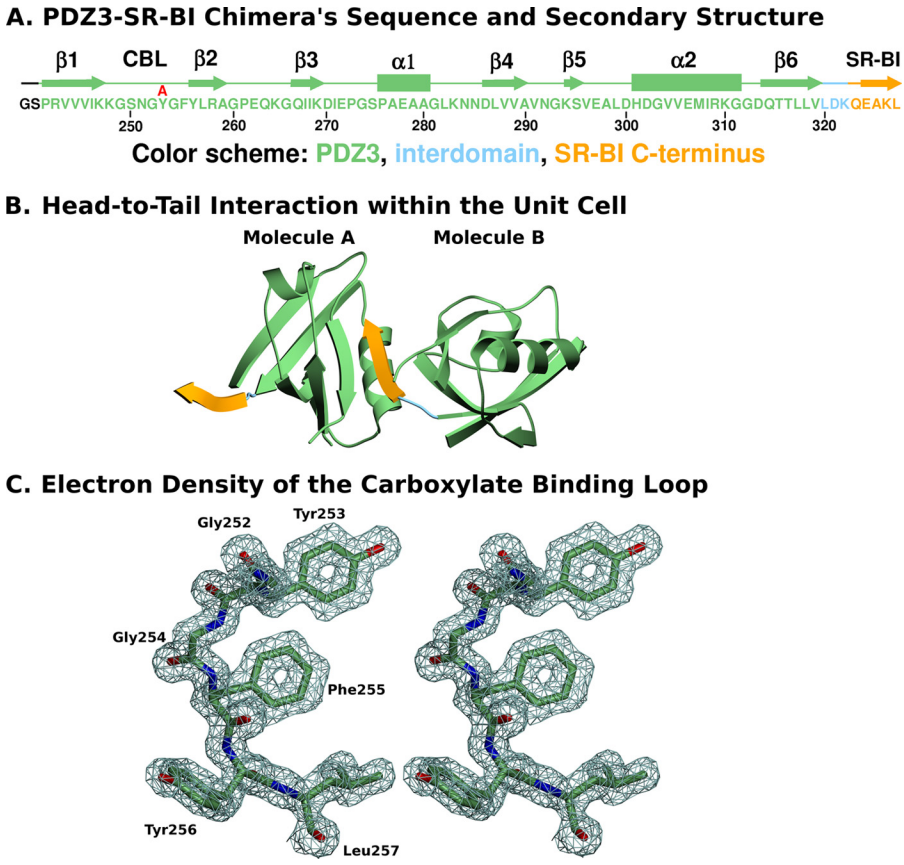

FIGURE 4. **X-ray crystal structure of the PDZ3-SR-BI target peptide chimera.** *A*, amino acid sequence of the recombinant chimeric protein used for crystallization: N-terminal Gly-Ser dipeptide derived from the cloning vector (*black*), PDZ3 domain (residues 241–319 (PDZK1 numbering), *green*), partial interdomain segment (320–322, lies between the PDZ3 and PDZ4 domains, *blue*), and 5 carboxyl-terminal residues of SR-BI (^{505}QEAKL^{509}, SR-BI numbering, *yellow*). Regions of secondary structure (β strands and α helices) and the CBL are indicated *above* the sequence, as is the single amino acid substitution (Tyr^{253} → Ala) examined in this study (*red*). *B*, unit cell representation showing the head-to-tail arrangement of two PDZ3-SR-BI target peptide chimeric molecules. This figure was generated using POVScript (34) and the color scheme in *panel A*. *C*, stereo view of the electron density map (contoured at 2.2 σ) and associated molecular model of a portion of the CBL (residues 252–257) at 1.50-Å resolution.

Phe^{255} of the CBL and, through water (W1–4)-mediated interactions, is connected to the carbonyl oxygens of Ile^{308} (α2) and Gly^{312}, and the side chain of Arg^{309} (α2). In addition, the hydroxyl group of Tyr^{253} (CBL) is connected via water-mediated hydrogen bonds with the carbonyl oxygens of Ile^{308} (α2), Arg^{309} (α2), and Gly^{312} (α2), thus interconnecting multiple segments of PDZ3 and the SR-BI peptide (Fig. 5, *B* and *C*). The amide nitrogen of Leu^{0} makes a hydrogen bond to the carbonyl

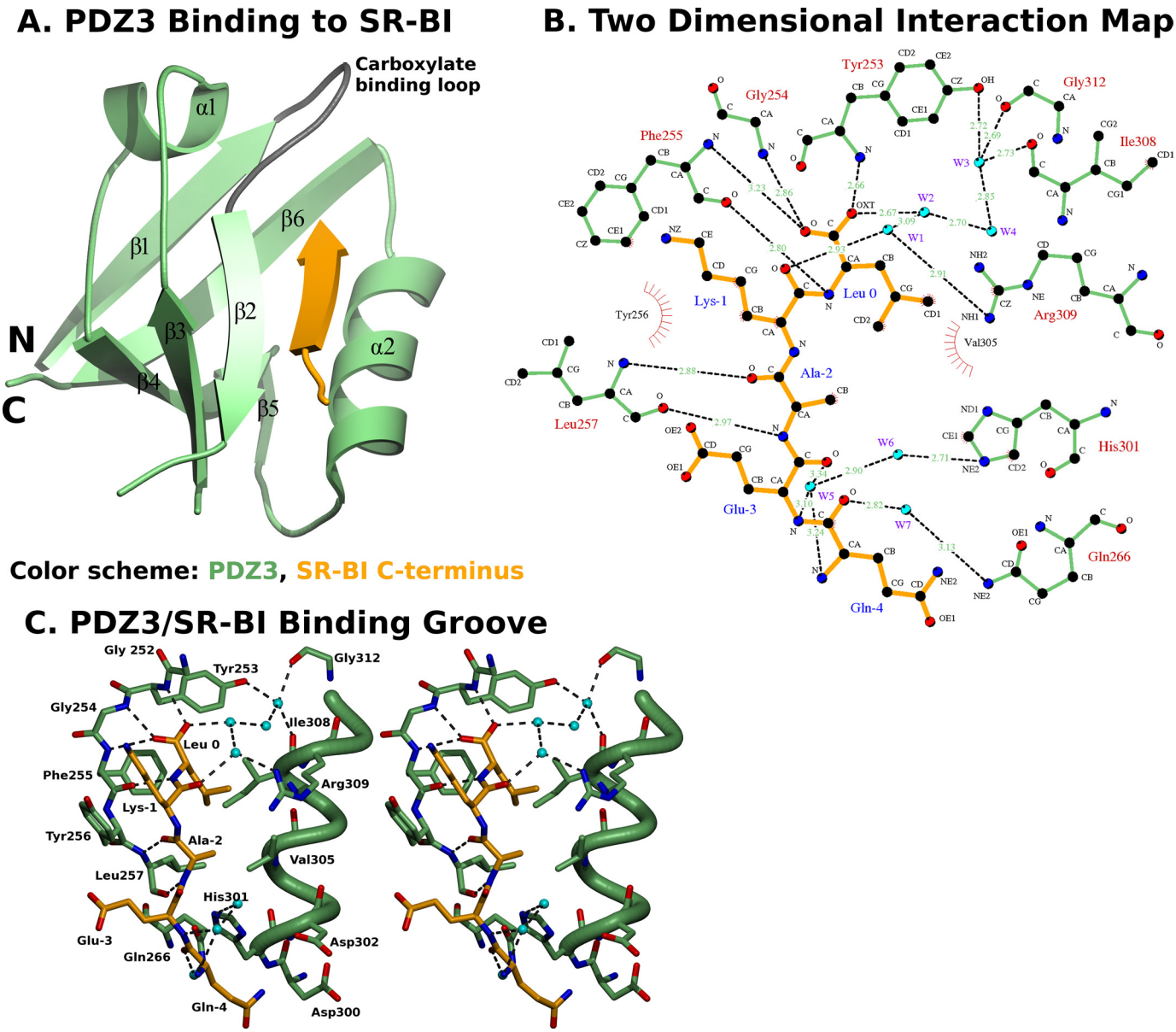

FIGURE 5. **Structure of the C-terminal SR-BI target peptide binding to PDZ3.** *A*, ribbon diagram showing the three-dimensional structure of PDZ3 (residues 241–319, *green with gray* carboxylate binding loop) and the bound C terminus of SR-BI ($^{-4}$QEAKL^{0}, *yellow*) from an adjacent molecule. The six β-strands (β1–β6), two α-helices (α1–α2), and carboxylate binding loop (*dark gray*) are indicated. The vector-derived residues are not shown. *B*, two-dimensional representation of interactions between PDZ1 (*green*) and the C-terminal SR-BI target peptide (*yellow*). Water molecules (W1, W2, etc.) are shown as *cyan spheres*. Hydrogen bonds are shown as *dashed lines* and hydrophobic interactions as arcs with *radial spokes*. This figure was generated using LIGPLOT (35). *C*, stereo representation of the ligand-binding groove of PDZ3 (*green*) and the SR-BI target peptide (*yellow*). Oxygen atoms, nitrogen atoms, and waters are shown in *red*, *dark blue*, and *cyan*, respectively. Hydrogen bonds are shown as *dashed lines*. The orientation is similar to that in *panel A*.

oxygen of Phe^{255} (CBL). The isobutyl side chain of Leu^{0} fits into a deep hydrophobic pocket composed of the side chains of Phe^{255} (CBL), Leu^{257} (CBL), Val^{305} (α2), Ile^{308} (α2), and Arg^{309} (α2) (Fig. 5, *B* and *C*)). There are also hydrogen bonds between the nitrogen and the carboxyl group of the Ala^{-2} target peptide and the carboxyl group and the amide nitrogen of Leu^{257} (CBL), respectively. The carbonyl oxygen of the Lys^{-1} peptide makes a water-mediated interaction with the side chain of Arg^{309} (α2) (Fig. 5, *B* and *C*). There is a hydrophobic interaction between the Cβ of Ala^{-2} (target peptide) and the isopropyl side chain of Val^{305} (α2). The amino and carbonyl groups of Glu^{-3} interact via water-mediated hydrogen bonds with the side chain of His^{301} and the carbonyl group of Gln^{-4} connects via a water-mediated hydrogen bond with the side chain of Gln^{266} (Fig. 5, *B* and *C*). The structure helps explain the virtually complete loss of target peptide binding by the Tyr^{253} → Ala substitution. There are several potential explanations based on the structure for why the side chain of Tyr^{253} (CBL) is essential for binding. The hydroxyl group forms water (W3)-mediated interactions with the backbones of Gly^{312} and Ile^{308} (α2) and is also involved in an elaborate network of water-mediated hydrogen bonding linking to the side chain of Arg^{309} (α2) and the carboxylate Leu^{0} of the target peptide (Fig. 5, *B* and *C*). It is also possible that substitution of the large side chain of Tyr^{253} with the smaller side chain of Ala leads to deleterious conformational changes in the binding site. We have previously shown that an equivalent

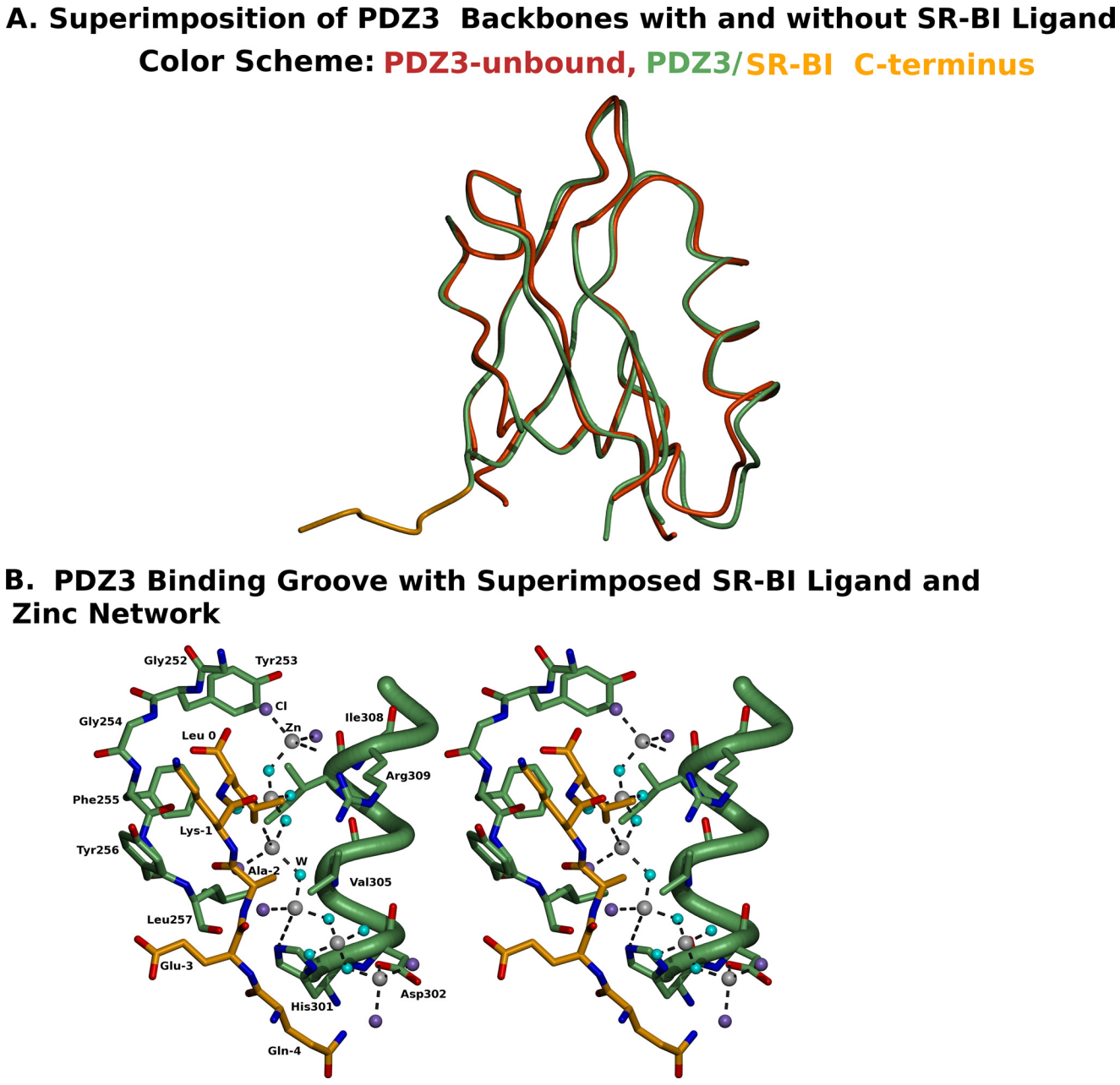

FIGURE 6. **Superimposition of the structures of PDZ3 determined with and without bound SR-BI target peptide.** *A*, the PDZ3-SR-BI target peptide chimera is labeled *green* (PDZ3) and *yellow* (SR-BI target peptide), and the unbound PDZ3 backbone structure is labeled *red*. *B*, stereo representation of the binding groove of PDZ3 (*green*) and the bound SR-BI target peptide (*yellow*), together with the zinc-chloride-water network seen in the target peptide free PDZ3 structure (zinc, *gray spheres*; chloride, *violet spheres*; and water, *cyan spheres*).

Tyr → Ala substitution in the PDZ1 domain also inhibits target peptide binding but does not dramatically alter the conformation of the domain as assessed by circular dichroism (18).

The superposition of the two independent structures of PDZ3, with and without its target SR-BI C-terminal peptide (Fig. 6*A*), showed that both structures are similar, sharing the characteristic conformation of typical PDZ domains (root mean square deviation of 0.68 Å for main chain atoms of residues 240 to 320); although there were some residues that exhibited substantial differences (*e.g.* the differences in positions for the Cα carbons of residues 255–256 (CBL), 260, 282–285, and 296–301 varied between 0.80 and 1.34 Å). This may be due to the fact that the ligand binding groove of PDZ3 is occupied in both structures either by the zinc-chloride-water network in the absence of the target peptide or by the C-terminal peptide of SR-BI ($^{-4}$QEAKL^{0}). As shown in the stereo diagram in Fig. 6*B*, the zinc-chloride-water chain runs adjacent and parallel to the position of the target peptide in the ligand binding groove of PDZ3 between the α2 and β2 strands. As a consequence, association of the zinc-chloride network with PDZ3 would prevent target peptide binding to PDZ3 and thus might represent a novel mode of regulation of ligand binding to PDZ domains *in vivo*.

The interactions between the C-terminal peptide of SR-BI and its binding site in PDZ3 are similar, but not identical, to those mediating the binding of this peptide to PDZ1 (18). The

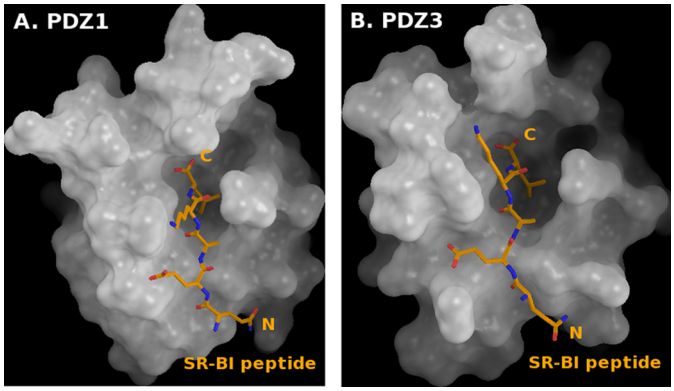

FIGURE 7. **Surface topology of PDZ1 (*A*) and PDZ3 (*B*) and their bound target peptides.** Surfaces of PDZ1 and PDZ3 (*gray*) are shown with their bound SR-BI target peptides ($^{-4}$QEAKL^{0}, stick representations with the amino and carboxyl termini labeled *N* and *C*). The Leu^{0} side chain hydrophobic binding pockets can be seen as deep cavities near the C termini of the target peptides. This figure was generated using PyMOL (36).

target peptide binding of SR-BI to PDZ3 is characterized by 12 hydrogen bounds and 4 hydrophobic interactions (Fig. 5*B*) (compared with 16 hydrogen bounds and 9 hydrophobic interactions between the C-terminal peptide of SR-BI and PDZ1) (18). Fig. 7 compares the surface topologies of the PDZ1 and PDZ3 domains of PDZK1 and their binding to the C-terminal peptide of SR-BI. The peptide adopts different conformations when bound to these PDZ domains. In addition, the hydrophobic pocket of PDZ3 appears wider than that of PDZ1. These findings may explain, at least in part, why the C terminus of SR-BI binds more tightly to PDZ1 than to PDZ3 (Fig. 1).

Role of PDZ3 in the Control of PDZK1 of Hepatic SR-BI Expression and Lipoprotein Metabolism in Vivo—We next compared the *in vivo* functional consequences of inactivating, in full-length PDZK1, the target peptide binding capacity of PDZ1 (Tyr^{20} → Ala) and PDZ3 (Tyr^{253} → Ala), either individually or in combination. Wild-type (WT) and *PDZK1* homozygous null knock-out (*PDZK1* KO) mice expressing essentially liver-specific *PDZK1* transgenes (Tg) were generated and characterized. We have previously described mice expressing the [Tyr^{20} → Ala]Tg (PDZ1) (18). In addition to the mice expressing these mutant transgenes ([Tyr^{20} → Ala]Tg (18), [Tyr^{253} → Ala]Tg, and [Tyr^{20} → Ala + Tyr^{253} → Ala]Tg), we studied as controls mice expressing PDZK1 mutants in which Ala was substituted for either Tyr or Phe at equivalent positions in the PDZ2 and PDZ4 domains (Phe^{145} → Ala-Tg or Tyr^{388} →Ala-Tg, respectively). The PDZ2 and PDZ4 domains do not exhibit detectable binding to the C-terminal peptide of SR-BI (Fig. 1, *B* and *E*). Two founder lines for *PDZK1*[Phe^{145} → Ala] (designated 3212 and 3215), one founder line for *PDZK1*[Tyr^{253} → Ala] (3342), two founder lines for *PDZK1*[Tyr^{388} → Ala] (3205 and 3344), and three founder lines for *PDZK1*[Tyr^{20} → Ala + Tyr^{253} → Ala] (8057, 8058, and 8226) were produced and used to generate matched wild-type (WT-Tg) and *PDZK1* KO (KO-Tg) transgenic mice on a mixed FVB/129SvEv background. Background matched nontransgenic WT and *PDZK1* KO mice were used as controls for each founder.

For each group of WT-Tg and KO-Tg mice and their nontransgenic controls, we determined the hepatic expression levels of PDZK1 and SR-BI proteins by quantitative immunoblot-

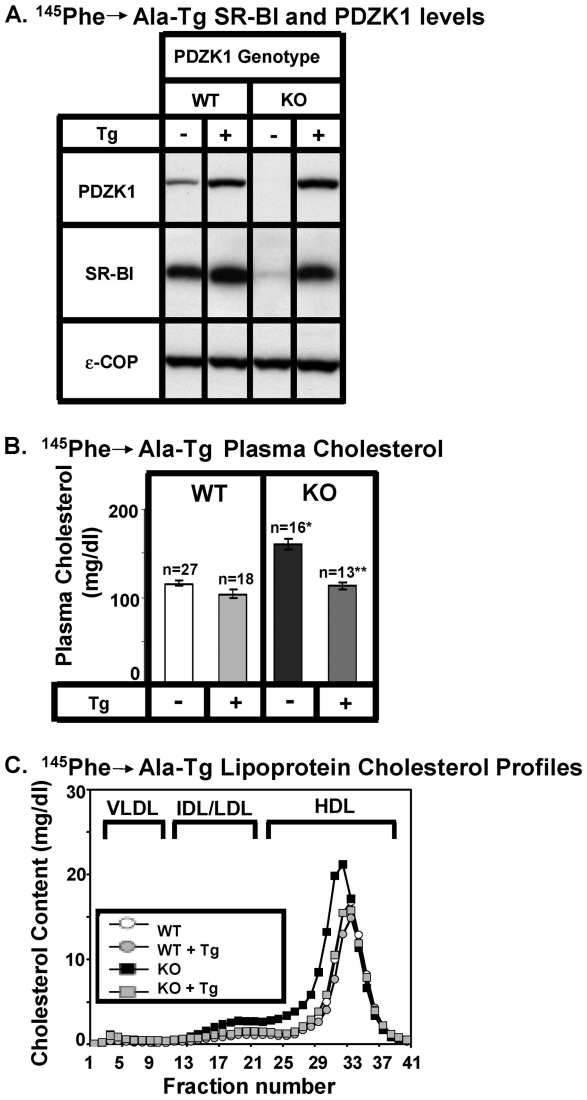

FIGURE 8. **Effects of expression of the *PDZK1*[Phe^{145} → Ala] transgene on hepatic SR-BI protein levels (*A*) and plasma lipoprotein cholesterols (*B* and *C*) in WT and *PDZK1* KO mice.** *A*, liver lysates (~30 μg of protein) from mice with the indicated genotypes, with (+) or without (−) the *PDZK1*[Phe^{145} → Ala]Tg (substitution in the PDZ2 domain), were analyzed by immunoblotting, and bands representing PDZK1 (~70 kDa) and SR-BI (~82 kDa) were visualized by chemiluminescence. ε-COP (~34 kDa) was used as a loading control. Note the faint SR-BI band in the nontransgenic *PDZK1* KO lane. Replicate experiments with multiple exposures and sample loadings were used to determine the relative levels of expression of SR-BI (Table 2). *B*, plasma samples were harvested from mice with the indicated genotypes and *PDZK1*[Phe^{145} → Ala]transgene. Total plasma cholesterol levels were determined in individual samples by enzymatic assay, and mean values from the indicated numbers of animals (*n*) are shown for each genotype. Independent WT and KO control animals for each founder line were generated to ensure that the mixed genetic backgrounds for experimental and control mice were matched. *Asterisk* indicates the nontransgenic KO plasma cholesterol levels were statistically significantly different from those plasma cholesterol levels of WT ($p < 0.0001$). **, indicates *PDZK1* KO [Phe^{145} → Ala]Tg plasma cholesterol levels were statistically significantly different from those plasma cholesterol levels of nontransgenic *PDZK1* KO mice ($p < 0.0001$). WT, WT [Phe^{145} → Ala]Tg, and KO [Phe^{145} → Ala]Tg plasma cholesterol levels were not statistically significantly different. *C*, plasma samples (described in *panel B*) from individual animals were size fractionated by FPLC, and the total cholesterol content of each fraction was determined by an enzymatic assay. The chromatograms are representative of multiple individually determined profiles. Approximate elution positions of native VLDL, IDL/LDL, and HDL particles are indicated by *brackets* and determined as previously described (7).

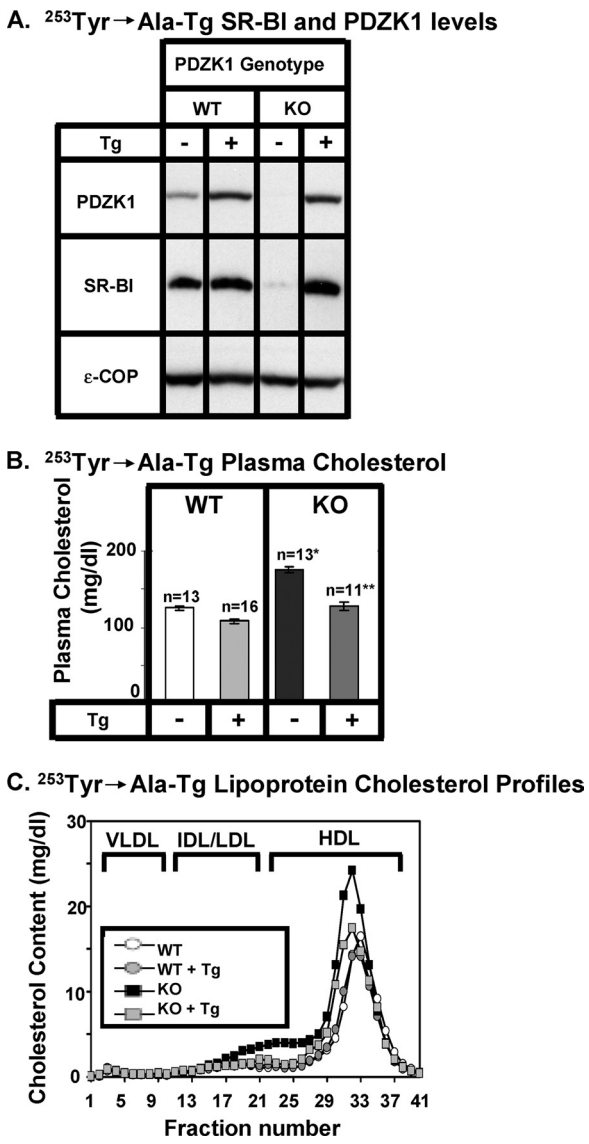

FIGURE 9. **Effects of expression of the *PDZK1*[Tyr^{253} → Ala]transgene on hepatic SR-BI protein levels (*A*) and plasma lipoprotein cholesterols (*B* and *C*) in WT and *PDZK1* KO mice.** *A*, liver lysates (~30 μg of protein) from mice with the indicated genotypes, with (+) or without (−) the *PDZK1*[Tyr^{253} → Ala]Tg (substitution in the PDZ3 domain), were analyzed by immunoblotting, and bands representing *PDZK1* (~70 kDa) and SR-BI (~82 kDa) were visualized by chemiluminescence. ε-COP (~34 kDa) was used as a loading control. Note the faint SR-BI band in the nontransgenic *PDZK1 KO* lane. Replicate experiments with multiple exposures and sample loadings were used to determine the relative levels of expression of SR-BI. *B*, plasma samples were harvested from mice with the indicated genotypes and *PDZK1*[Tyr^{253} → Ala]-transgene. Total plasma cholesterol levels were determined in individual samples by enzymatic assay, and mean values from the indicated numbers of animals (*n*) are shown for each genotype. Independent WT and KO control animals for the founder line were generated to ensure that the mixed genetic backgrounds for experimental and control mice were matched. * indicates the nontransgenic KO plasma cholesterol levels were statistically significantly different from those plasma cholesterol levels of WT ($p < 0.0001$). ** indicates *PDZK1* KO [Tyr^{253} → Ala]Tg plasma cholesterol levels were statistically significantly different from those plasma cholesterol levels of nontransgenic *PDZK1* KO mice ($p < 0.0001$). WT, WT [Tyr^{253} → Ala]Tg, and KO [Tyr^{253} → Ala]Tg plasma cholesterol levels were not statistically significantly different. *C*, plasma samples (described in *panel B*) from individual animals were size fractionated by FPLC, and the total cholesterol content of each fraction was determined by an enzymatic assay. The chromatograms are representative of multiple individually determined profiles. Approximate elution positions of native VLDL, IDL/LDL, and HDL particles are indicated by *brackets* and determined as previously described (7).

ting (*panels A* in Figs. 8-11, ε-COP was used as a loading control). The ratios of band intensities (transgenic/nontransgenic) are shown in Table 2. The relative steady state levels of *PDZK1* transgene-encoded proteins varied between 2.4 ± 0.5- and 29.2 ± 3.9-fold greater than that of endogenous PDZK1 in nontransgenic WT mice. Thus, for all experiments described below there was substantial overexpression of the transgene-encoded PDKZ1 proteins relative to that of the endogenous PDZK1 protein in nontransgenic WT mice. We also measured plasma total cholesterol levels (*panels B* in Figs. 8–11), the size distribution of plasma lipoproteins (FPLC lipoprotein cholesterol profiles, *panels C* in Figs. 8–11), and the distribution of SR-BI protein in hepatocytes *in vivo* (immunohistochemistry, Fig. 12).

Effects of Mutant PDZK1 Constructs in Wild-type Mice—In transgenic WT mice relative to nontransgenic WT mice, expression of each mutant PDZK1 protein had virtually no influence on the levels of hepatic SR-BI protein expression determined by immunoblotting (*panels A* in Figs. 8–11 and Table 2), nor did the transgenes alter sinusoidal membrane-associated distribution of SR-BI determined by immunohistochemistry (Fig. 12, *panels A*, *C*, *E*, *G*, and *I*), plasma cholesterol levels (*left panels B* in Figs. 8–11), or lipoprotein cholesterol size distribution profiles determined by FPLC (*circles* in *panels C* of Figs. 8–11)). Similar results have been reported for the [Tyr^{20} → Ala]Tg in WT mice (18). Thus, these mutated transgenes did not produce a dominant-negative effect when expressed in WT mice (an example of a dominant-negative construct is described in Ref. 17).

Effects of Mutant PDZK1 Constructs in PDZK1 KO Mice—As previously described (5, 16, 17, 28), absence of PDKZ1 expression in non-transgenic *PDZK1* KO mice resulted in a dramatic loss of hepatic SR-BI protein (*panels A* in Figs. 8–11 and Fig. 12*B*), increased plasma total cholesterol (*black bars* in *right panels B* in Figs. 8–11), and an increase in the size of HDL particles (leftward shift in lipoprotein profiles, *black squares* in *panels C* in Figs. 8–11). All of these abnormalities are corrected by hepatic expression of a wild-type *PDZK1* transgene in otherwise PDKZ1 knock-out animals (17). Hepatic transgenic expression of the *PDZK1*[Phe^{145} → Ala], *PDZK1*[Tyr^{253} → Ala], and *PDZK1*[Tyr^{388} → Ala] mutants in *PDZK1* KO mice corrected all of these abnormalities (Figs. 8–10, Fig. 12*D*, *F* and *H*, and Table 2). Thus, as illustrated in PDZK1 mice with an ~3-fold overexpression of *PDZK1*[Tyr^{253} → Ala] (Fig. 9), the ability of PDZ3 to bind to the C terminus of SR-BI was not required for essentially full normalization of hepatic SR-BI steady state expression, localization, and function.

We have previously reported that hepatic transgenic overexpression (~10–20-fold) of *PDZK1*[Tyr^{20} → Ala] restored in *PDZK1* KO mice normal levels of hepatic SR-BI protein, substantial amounts of which were on hepatocyte plasma membranes, and partially corrected plasma cholesterol levels with a modest reduction in the amounts of abnormally large, plasma lipoproteins (18). In marked contrast, hepatic transgenic overexpression (~2–4-fold) of the doubly substituted *PDZK1*[Tyr^{20} → Ala + Tyr^{253} → Ala]transgene was unable to complement the major abnormalities exhibited by PDZK1 KO mice, including high plasma cholesterol level, abnormal lipo-

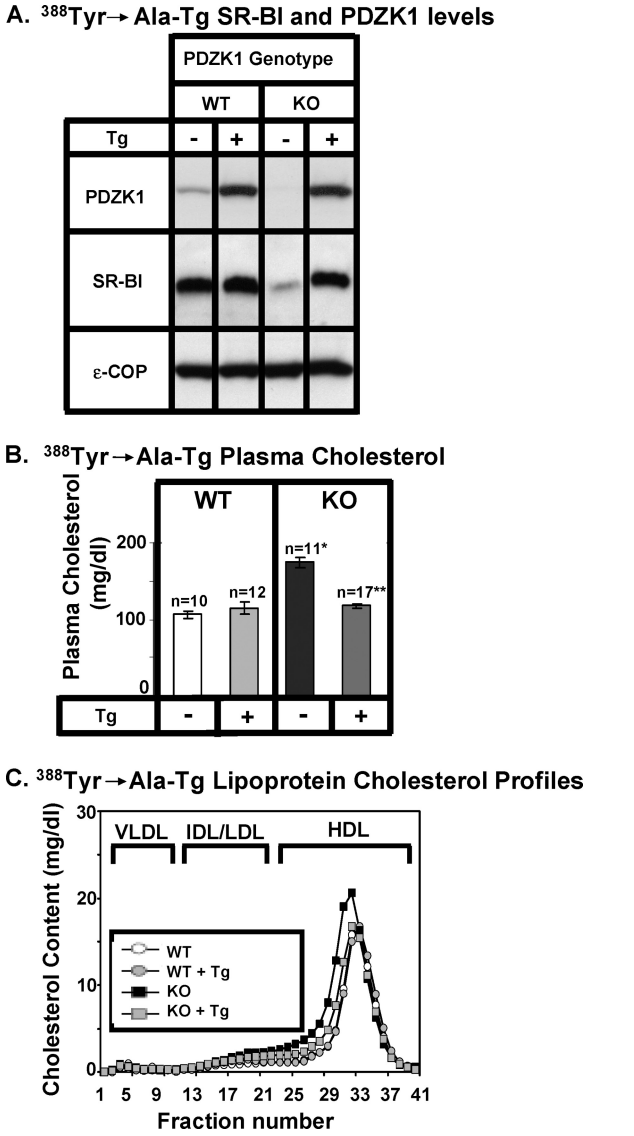

FIGURE 10. **Effects of expression of the *PDZK1*[Tyr^{388} → Ala]transgene on hepatic SR-BI protein levels (*A*) and plasma lipoprotein cholesterols (*B* and *C*) in WT and *PDZK1* KO mice.** *A*, liver lysates (~30 μg of protein) from mice with the indicated genotypes, with (+) or without (−) the *PDZK1*[Tyr^{388} → Ala]Tg (substitution in the PDZ4 domain), were analyzed by immunoblotting, and bands representing PDZK1 (~70 kDa) and SR-BI (~82 kDa) were visualized by chemiluminescence. ε-COP (~34 kDa) was used as a loading control. Note the faint SR-BI band in the nontransgenic *PDZK1* KO lane. Replicate experiments with multiple exposures and sample loadings were used to determine the relative levels of expression of SR-BI. *B*, plasma samples were harvested from mice with the indicated genotypes and *PDZK1*[Tyr^{388} → Ala]-transgene. Total plasma cholesterol levels were determined in individual samples by enzymatic assay, and mean values from the indicated numbers of animals (*n*) are shown for each genotype. Independent WT and KO control animals for each founder line were generated to ensure that the mixed genetic backgrounds for experimental and control mice were matched. * indicates the nontransgenic KO plasma cholesterol levels were statistically significantly different from those plasma cholesterol levels of WT ($p < 0.0001$). ** indicates *PDZK1* KO ([Tyr^{388} → Ala]Tg) plasma cholesterol levels were statistically significantly different from those plasma cholesterol levels of nontransgenic *PDZK1* KO mice ($p < 0.0001$). WT, WT ([Tyr^{388} → Ala]Tg), and KO ([Tyr^{388} → Ala]Tg) plasma cholesterol levels were not statistically significantly different. *C*, plasma samples (described in *panel B*) from individual animals were size fractionated by FPLC, and the total cholesterol content of each fraction was determined by an enzymatic assay. The chromatograms are representative of multiple individually determined profiles. Approximate elution positions of native VLDL, IDL/LDL, and HDL particles are indicated by *brackets* and determined as previously described (7).

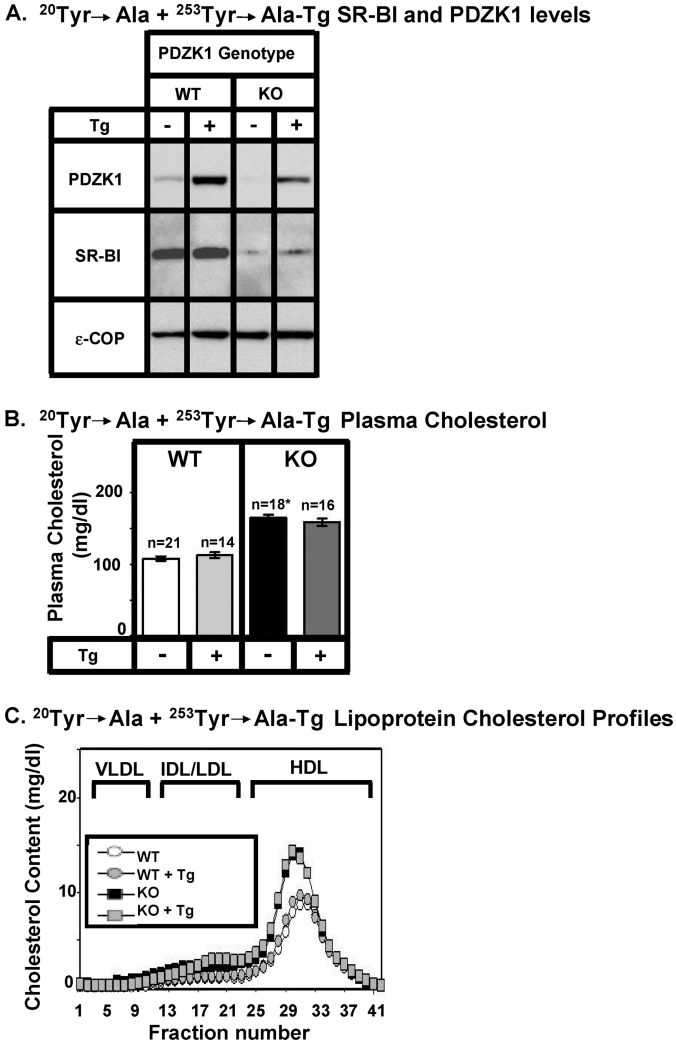

FIGURE 11. **Effects of expression of the *PDZK1*[Tyr^{20} → Ala + Tyr^{253} → Ala] double mutant transgene on hepatic SR-BI protein levels (*A*) and plasma lipoprotein cholesterols (*B* and *C*) in WT and *PDZK1* KO mice.** *A*, liver lysates (~30 μg of protein) from mice with the indicated genotypes, with (+) or without (−) the *PDZK1*[Tyr^{20} → Ala + Tyr^{253} → Ala]Tg (substitutions in the PDZ1 and PDZ3 domains), were analyzed by immunoblotting, and bands representing PDZK1 (~70 kDa) and SR-BI (~82 kDa) were visualized by chemiluminescence. ε-COP (~34 kDa) was used as a loading control. Note the faint SR-BI band in the nontransgenic *PDZK1* KO and the *PDZK1* KO expressing the *PDZK1*[Tyr^{20} → Ala + Tyr^{253} → Ala]Tg lanes. Replicate experiments with multiple exposures and sample loadings were used to determine the relative levels of expression of SR-BI. *B*, plasma samples were harvested from mice with the indicated genotypes and *PDZK1*[Tyr^{20} → Ala + Tyr^{253} → Ala]transgene. Total plasma cholesterol levels were determined in individual samples by enzymatic assay, and mean values from the indicated numbers of animals (*n*) are shown for each genotype. Independent WT and KO control animals for each founder line were generated to ensure that the mixed genetic backgrounds for experimental and control mice were matched. * indicates the nontransgenic KO plasma cholesterol levels were statistically significantly different from those plasma cholesterol levels of WT ($p < 0.0001$). *PDZK1* KO (Tyr^{20} → Ala + Tyr^{253} → Ala) plasma cholesterol levels were not statistically significantly different from those plasma cholesterol levels of nontransgenic *PDZK1* KO mice. WT and WT (Tyr^{20} → Ala + Tyr^{253} → Ala) plasma cholesterol levels were not statistically significantly different. *C*, plasma samples (described in *panel B*) from individual animals were size fractionated by FPLC, and the total cholesterol content of each fraction was determined by an enzymatic assay. The chromatograms are representative of multiple individually determined profiles. Approximate elution positions of native VLDL, IDL/LDL, and HDL particles are indicated by *brackets* and determined as previously described (7).

TABLE 2
PDZK1 and SR-BI protein expression levels in transgenic mice expressing PDZK1 transgenic mutants (Tg) relative to non-transgenic wild-type (WT) controls

PDZK1 mutant	Founder	Relative PDZK1 protein level, WT-Tg/WT	Relative SR-BI protein level	
			WT-Tg/WT	KO-Tg/WT
$Phe^{145} \rightarrow Ala$	3212	7.60 ± 1.82^a	1.31 ± 0.12^b	1.48 ± 0.44^b
	3215	10.80 ± 1.91^a		
$Tyr^{253} \rightarrow Ala$	3342	2.91 ± 0.60^a	0.96 ± 0.05^b	1.15 ± 0.54^b
$Tyr^{388} \rightarrow Ala$	3205	29.25 ± 3.88^a	1.37 ± 0.20^b	1.48 ± 0.38^b
	3344	18.19 ± 4.58^a		
$Tyr^{20} \rightarrow Ala + Tyr^{253} \rightarrow Ala$	8057	3.91 ± 0.56^a	1.05 ± 0.13^b	0.17 ± 0.05^c
	8058	2.44 ± 0.49^a		
	8226	2.58 ± 0.43^a		

[a] $p < 0.05$ between WT-Tg and WT.
[b] $p > 0.05$ between WT-Tg or KO-Tg and WT.
[c] $p < 0.05$ between KO-Tg and WT.

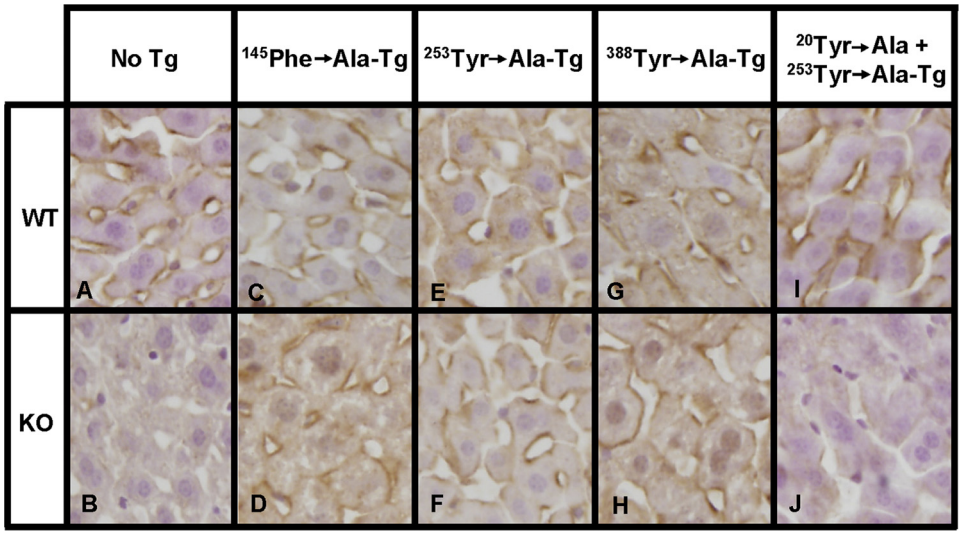

FIGURE 12. **Immunohistochemical analysis of hepatic SR-BI in WT and *PDZK1* KO nontransgenic (*A* and *B*), *PDZK1*[$Phe^{145} \rightarrow Ala$]transgenic (*C* and *D*), *PDZK1*[$Tyr^{253} \rightarrow Ala$]transgenic (*E* and *F*), *PDZK1*[$Tyr^{388} \rightarrow Ala$]transgenic (*G* and *H*), and *PDZK1*[$Tyr^{20} \rightarrow Ala + Tyr^{253} \rightarrow Ala$]transgenic (*I* and *J*) mice.** Livers from mice of the indicated genotypes and Tg were fixed, frozen, and sectioned. The sections were then stained with a polyclonal anti-SR-BI antibody and a biotinylated anti-rabbit IgG secondary antibody and visualized by immunoperoxidase staining (magnification ×600).

protein profile, and absence of substantial cell-surface SR-BI in hepatocytes (Figs. 11 and 12, *B* and *J*). There was a minor increase in SR-BI protein expression from 8% WT in *PDZK1* KO to 17% WT in *PDZK1* KO mice with the *PDZK1*[$Tyr^{20} \rightarrow Ala + Tyr^{253} \rightarrow Ala$]transgene. Thus, the ability of *PDZK1*[$Tyr^{20} \rightarrow Ala$] to bind SR-BI via PDZ3 and *PDZK1*[$Tyr^{253} \rightarrow Ala$] to bind SR-BI via PDZ1 results in functional hepatic PDZK1 *in vivo*, whereas the double mutant *PDZK1*[$Tyr^{20} \rightarrow Ala + Tyr^{253} \rightarrow Ala$] that cannot bind the C terminus of SR-BI (Fig. 2*C*) is essentially inactive *in vivo*.

DISCUSSION

PDZK1 is a four PDZ domain-containing adaptor protein responsible for maintaining normal hepatic expression, localization, and function of the HDL receptor SR-BI (5). Initial (14) and subsequent (15, 17, 18) studies have shown that the N-terminal PDZ1 domain of PDZK1 binds the C terminus of SR-BI via its canonical PDZ domain target peptide binding site. Although an early report suggested that PDZ1 was the only PDZ domain in PDKZ1 that binds the C terminus of SR-BI (14), we found that hepatic overexpression in *PDZK1* KO mice of a mutant *PDZK1* transgene in which the PDZ1 domain was inactivated ($Tyr^{20} \rightarrow Ala$ substitution) could partially or fully correct the characteristic SR-BI and lipoprotein abnormalities of the *PDZK1* KO mice (18). This finding raised the possibility that there may be additional binding sites within PDZK1 that bind SR-BI. Those sites might mediate a productive SR-BI/PDZK1 interaction that was previously attributed exclusively to the canonical binding of the C terminus of SR-BI to PDZ1.

We have used a combination of *in vitro* and *in vivo* approaches to characterize an additional binding site for the C terminus of SR-BI on PDZK1. We found that the C-terminal heptapeptide of SR-BI binds to the PDZ3 domain of PDZK1 ($K_d = 37.0\ \mu M$), albeit with a lower affinity than PDZ1 ($K_d = 3.6\ \mu M$), but not to either the PDZ2 or PDZ4 domains (Fig. 1). A $Tyr^{253} \rightarrow Ala$ substitution in the CBL of PDZ3 blocked detectable binding of the SR-BI C-terminal peptide, as does the analogous $Tyr^{20} \rightarrow Ala$ substitution in PDZ1 (18). To understand the structural bases of these results, we determined the high resolution (1.5 Å) crystal structure of a chimeric recombinant protein comprising PDZ3 (residues 241–319 of wild-type PDZK1) and 3 amino acids from the interdomain region between PDZ3 and PDZ4 (residues 320–322) that was extended at its C terminus by addition of the 5 carboxyl-terminal residues of its target peptide from the C terminus of SR-BI:

^{505}QEAKL^{509}. In the crystals, the SR-BI target peptide from one molecule binds in the peptide binding groove between the α2 helix and β2 strand of the PDZ3 portion of an adjacent molecule, resulting in an infinite chain of head-to-tail molecules. The target peptide and the α2 helix, β2 strand, and CBL of PDZ3, particularly Tyr^{253}, form an extensive direct and water-mediated hydrogen bond network (Figs. 4 and 5), disruption of which by the Tyr^{253} → Ala substitution may contribute to the loss of target peptide binding (Figs. 1 and 2, also see Ref. 18). Comparison of the structures of the target peptide binding of SR-BI to PDZ3 (this work) and PDZ1 (18) show that target peptide binding to PDZ3 is characterized by (i) a less extensive water-hydrogen bond network and fewer hydrophobic interactions, (ii) a somewhat different orientation of the side chains of the target peptide, and (iii) a wider hydrophobic pocket in PDZ3 into which the side chain of Leu^{509} binds (Figs. 5 and 7, and Ref. 18). These differences appear to account for the lower binding affinity of the C-terminal heptapeptide of SR-BI to PDZ3 than to PDZ1 (Figs. 1 and 2, and Ref. 18).

We also determined the high resolution (1.3 Å) structure of PDZ3 in the absence of the target peptide. The conformation of PDZ3 without bound peptide was almost identical to that with the bound peptide and similar to the PDZ-fold reported previously for several PDZ domains, including PDZ1 of PDZK1 (18, 29, 32). Crystals of the target peptide-free PDZ3 were grown from a solution containing 0.2 M zinc and 75 mM NaCl. Strikingly, the peptide-binding groove was occupied by an extensive zinc-chloride-water chain (Fig. 3) that mediated the dimerization of symmetry-related PDZ3 domains in the crystal lattice. The position of this chain in the groove was parallel to and slightly displaced from that of the target peptide in the peptide-bound structure. As a consequence, association of the zinc-chloride network with PDZ3 would prevent target peptide binding to PDZ3 and might represent a novel mode of metal regulation of ligand binding to PDZ domains *in vivo*. To our knowledge, such a role for zinc has not been described previously. It is noteworthy that LaLonde and Bretscher (33) have previously reported that PDZK1 can undergo modest homodimerization mediated by PDZ3; although it is not clear if metal ions played any role in the PDZ3-mediated homodimerization in that report.

We explored the role of the target peptide binding of PDZ3 on PDZK1-mediated regulation of SR-BI *in vivo*. We compared the abilities of hepatic overexpression of wild-type and mutant *PDZK1* transgenes to complement the SR-BI-related defects in *PDZK1* KO mice. These defects include dramatic loss of hepatic SR-BI protein expression and consequent abnormal lipoprotein metabolism (high plasma cholesterol carried in abnormally large HDL particles). We have previously reported that hepatic overexpression of wild-type *PDZK1* fully corrects these defects in *PDKZ1* KO mice (17). Inactivating PDZ3 binding to the C terminus of SR-BI with a Tyr^{253} → Ala substitution in an otherwise wild-type PDZK1 transgene did not prevent the transgene correcting all of these defects in *PDZK1* KO mice. Thus, SR-BI binding to the PDZ3 domain is not necessary for PDZK1 regulation of SR-BI, presumably because binding to the PDZ1 domain is sufficient.

We previously showed that a mutant *PDZK1* transgene with an inactivating mutation in PDZ1 (Tyr^{20} → Ala) can almost completely correct the SR-BI-related defects in *PDZK1* KO mice (18). The almost normal activity of the Tyr^{20} → Ala substituted PDZK1 was presumably a consequence of SR-BI/PDZK1 binding mediated by PDZ3. This conclusion was strongly supported by our analysis of *PDZK1* KO mice overexpressing an hepatic mutant *PDZK1* transgene with inactivating mutations in both PDZ1 and PDZ3 (double Tyr^{20} → Ala + Tyr^{253} → Ala substitution). The double mutant transgene did not correct the SR-BI-related defects, notably it did not restore normal SR-BI expression, localization, or function, as it did not correct the abnormal lipoprotein metabolism (Fig. 11 and 12). Thus, we conclude that PDZK1 regulation of hepatic SR-BI requires direct binding of the C terminus of SR-BI to either the PDZ1 or PDZ3 domain, and that binding to both domains simultaneously is not required for the hepatic, PDZK1-dependent SR-BI activities measured in this study. There may be other activities of PDZK1 that are dependent on simultaneous binding to PDZ1 and PDZ3, but those activities, if any, were not examined here. Future studies will be required to define in detail the molecular and cellular mechanisms underlying the influence of PDZK1 on hepatic SR-BI.

Acknowledgments—We thank Joel Lawitts from the Beth Israel Deaconess Medical Center transgenic facility for help generating the transgenic mice, Debby Pheasant from the MIT Biophysical Instrumentation Facility for helping with the ITC experiments, Verna Frasca from GE Healthcare for helping with the interpretation of the ITC data and the staff at beamline X12C, National Synchrotron Light Source (Brookhaven National Laboratory) for assistance during data collection. The crystal structures of PDZ3 were partially solved at the RapiData 2010 course.

REFERENCES

1. Pawson, T., and Nash, P. (2003) *Science* **300,** 445–452
2. van Ham, M., and Hendriks, W. (2003) *Mol. Biol. Rep.* **30,** 69–82
3. Kocher, O., and Krieger, M. (2009) *Curr. Opin. Lipidol.* **20,** 236–241
4. Yesilaltay, A., Kocher, O., Rigotti, A., and Krieger, M. (2005) *Curr. Opin. Lipidol.* **16,** 147–152
5. Kocher, O., Yesilaltay, A., Cirovic, C., Pal, R., Rigotti, A., and Krieger, M. (2003) *J. Biol. Chem.* **278,** 52820–52825
6. Rigotti, A., Miettinen, H. E., and Krieger, M. (2003) *Endocr. Rev.* **24,** 357–387
7. Rigotti, A., Trigatti, B. L., Penman, M., Rayburn, H., Herz, J., and Krieger, M. (1997) *Proc. Natl. Acad. Sci. U.S.A.* **94,** 12610–12615
8. Zhang, S. H., Reddick, R. L., Piedrahita, J. A., and Maeda, N. (1992) *Science* **258,** 468–471
9. Plump, A. S., Smith, J. D., Hayek, T., Aalto-Setälä, K., Walsh, A., Verstuyft, J. G., Rubin, E. M., and Breslow, J. L. (1992) *Cell* **71,** 343–353
10. Braun, A., Trigatti, B. L., Post, M. J., Sato, K., Simons, M., Edelberg, J. M., Rosenberg, R. D., Schrenzel, M., and Krieger, M. (2002) *Circ. Res.* **90,** 270–276
11. Kocher, O., Yesilaltay, A., Shen, C. H., Zhang, S., Daniels, K., Pal, R., Chen, J., and Krieger, M. (2008) *Biochim. Biophys. Acta* **1782,** 310–316
12. Trigatti, B., Rayburn, H., Viñals, M., Braun, A., Miettinen, H., Penman, M., Hertz, M., Schrenzel, M., Amigo, L., Rigotti, A., and Krieger, M. (1999) *Proc. Natl. Acad. Sci. U.S.A.* **96,** 9322–9327
13. Yesilaltay, A., Daniels, K., Pal, R., Krieger, M., and Kocher, O. (2009) *PLoS ONE* **4,** e8103
14. Ikemoto, M., Arai, H., Feng, D., Tanaka, K., Aoki, J., Dohmae, N., Takio, K., Adachi, H., Tsujimoto, M., and Inoue, K. (2000) *Proc. Natl. Acad. Sci. U.S.A.* **97,** 6538–6543
15. Silver, D. L. (2002) *J. Biol. Chem.* **277,** 34042–34047

16. Fenske, S. A., Yesilaltay, A., Pal, R., Daniels, K., Barker, C., Quiñones, V., Rigotti, A., Krieger, M., and Kocher, O. (2009) *J. Biol. Chem.* **284,** 5797–5806
17. Fenske, S. A., Yesilaltay, A., Pal, R., Daniels, K., Rigotti, A., Krieger, M., and Kocher, O. (2008) *J. Biol. Chem.* **283,** 22097–22104
18. Kocher, O., Birrane, G., Tsukamoto, K., Fenske, S., Yesilaltay, A., Pal, R., Daniels, K., Ladias, J. A., and Krieger, M. (2010) *J. Biol. Chem.* **285,** 34999–35010
19. Otwinowski, Z., and Minor, W. (1997) in *Methods in Enzymology* (Carter, C.W., and Sweet, R. M., eds) Vol. 276, pp. 307–326, Academic Press, New York
20. Sheldrick, G. M. (2008) *Acta Crystallogr. Sect. A* **64**, 112–122
21. McCoy, A. J., Grosse-Kunstleve, R. W., Adams, P. D., Winn, M. D., Storoni, L. C., and Read, R. J. (2007) *J. Appl. Crystallogr.* **40,** 658–674
22. Vagin, A. A., Steiner, R. A., Lebedev, A. A., Potterton, L., McNicholas, S., Long, F., and Murshudov, G. N. (2004) *Acta Crystallogr. D Biol. Crystallogr.* **60**, 2184–2195
23. Emsley, P., and Cowtan, K. (2004) *Acta Crystallogr. D Biol. Crystallogr.* **60,** 2126–2132
24. Kocher, O., Pal, R., Roberts, M., Cirovic, C., and Gilchrist, A. (2003) *Mol. Cell. Biol.* **23,** 1175–1180
25. Simonet, W. S., Bucay, N., Lauer, S. J., and Taylor, J. M. (1993) *J. Biol. Chem.* **268,** 8221–8229
26. Palmiter, R. D., and Brinster, R. L. (1986) *Annu. Rev. Genet.* **20,** 465–499
27. Guo, Q., Penman, M., Trigatti, B. L., and Krieger, M. (1996) *J. Biol. Chem.* **271,** 11191–11196
28. Yesilaltay, A., Kocher, O., Pal, R., Leiva, A., Quiñones, V., Rigotti, A., and Krieger, M. (2006) *J. Biol. Chem.* **281,** 28975–28980
29. Doyle, D. A., Lee, A., Lewis, J., Kim, E., Sheng, M., and MacKinnon, R. (1996) *Cell* **85,** 1067–1076
30. Von Ossowski, I., Oksanen, E., Von Ossowski, L., Cai, C., Sunberg, M., Goldman, A., and Keinänen, K. (2006) *FEBS J.* **273,** 5219–5229
31. Karthikeyan, S., Leung, T., and Ladias, J. A. (2001) *J. Biol. Chem.* **276,** 19683–19686
32. Karthikeyan, S., Leung, T., and Ladias, J. A. (2002) *J. Biol. Chem.* **277,** 18973–18978
33. LaLonde, D. P., and Bretscher, A. (2009) *Biochemistry* **48,** 2261–2271
34. Fenn, T., Ringe, D., and Petsko, G. (2003) *J. Appl. Crystallogr.* **36,** 944–947
35. Wallace, A. C., Laskowski, R. A., and Thornton, J. M. (1995) *Protein Eng.* **8,** 127–134
36. DeLano, W. (2002) *PyMol*, DeLano Scientific, San Carlos, CA